



# Evolution of drought characteristics and propagation from meteorological to agricultural drought under the influences of climate change and human activities

Liang Li<sup>1,2,3</sup> · Qing Peng<sup>1,2,3</sup> · Zongyang Li<sup>1,2,3</sup> · Huanjie Cai<sup>1,2,3</sup>

Received: 16 August 2023 / Accepted: 26 February 2024 / Published online: 8 March 2024  
© The Author(s), under exclusive licence to Springer-Verlag GmbH Germany, part of Springer Nature 2024

## Abstract

Understanding the propagation of agricultural droughts (AD) is important to comprehensively assess drought events and develop early warning systems. The present study aims to assess the impacts of climate change and human activities on drought characteristics and propagation from meteorological drought (MD) to AD in the Yellow River Basin (YRB) over the 1950–2021 period using the Standardized Precipitation Evapotranspiration Index (SPEI) and Standardized Soil Moisture Index (SSMI). In total, the YRB was classified into three groups of catchments for spring wheat and four groups of catchments for winter wheat based on different human influence degrees (HId). In addition, the entire study period was divided into periods with natural (NP), low (LP), and high (HP) impacts of human activities, corresponding to 1950–1971, 1972–1995, and 1996–2021, respectively. The results demonstrated the significance and credibility of the application of the natural and human-impacted catchment comparison method for drought characteristics and propagation from meteorological to agricultural drought in the YRB. Winter wheat showed a more pronounced drying trend than spring wheat under both MD and AD. The results showed meteorological drought intensity (MDI) and agricultural drought intensity (ADI) intensified for spring and winter wheat in NP, with correspondingly a short propagation time, followed by those in the LP and HP in catchments minimally impacted by human activities. On the other hand, increases in the MDI and ADI, as well as in their times, for both spring and winter wheat were observed from the LP to the HP in all catchments. The MDI, ADI, and their propagation times for winter wheat generally showed greater fluctuations than those for spring wheat. Human activities increasingly prolonged the drought propagation time. In contrast, climate change insignificantly shortened the drought propagation time.

**Keywords** Meteorological drought · Agricultural drought · Dynamic drought propagation · Climate change · Human activities

## Introduction

Drought is widely recognized as a complex multifaceted phenomenon (Van Loon 2015), characterized by obvious spatiotemporal patterns, particularly in semi-arid and arid areas (Wu et al. 2022). Drought events are caused by a deficiency of precipitation over an extended period, representing meteorological droughts (MD). The propagation of these drought events is governed by hydro-meteorological properties. The combined effect of severe water deficit, vapor pressure deficit, enhanced atmospheric evaporative demand, and reduced soil moisture contents can restrict optimal plant growth and production, resulting in agricultural droughts (AD) (Zhang et al. 2022). This phenomenon is referred to as drought propagation from MD to AD. This propagation is characterized by four elements, namely, pooling (MDs

Responsible Editor: Philippe Garrigues

✉ Huanjie Cai  
huanjiecai@yahoo.com

<sup>1</sup> Key Laboratory of Agricultural Soil and Water Engineering in Arid and Semiarid Areas, Ministry of Education, Northwest A&F University, Yangling 712100, Xianyang, China

<sup>2</sup> Institute of Water-Saving Agriculture in Arid Areas of China, Northwest A&F University, Yangling 712100, Xianyang, China

<sup>3</sup> College of Water Resources and Architectural Engineering, Northwest A&F University, Yangling 712100, Xianyang, China

are combined into a prolonged AD), attenuation (MDs are attenuated in the soil under relatively high soil water contents), lag (a lag occurs between meteorological and AD), and lengthening (drought periods become longer, moving from meteorological to AD) (Van Loon and Van Lanen 2012). Indeed, numerous researchers have investigated the drought propagation characteristics using several approaches and taking into account drought processes and their controlling factors. These factors include climatic conditions, teleconnection factors (e.g., sea surface temperature and solar activities), catchment soil properties, geographic characteristics, land use types, and human activities (Bonfils et al. 2020; Samaniego et al. 2018; Van Langen et al. 2021; Wu et al. 2022).

Global warming and climate change have greatly influenced the development, management, and planning of surface and groundwater resources (Singh et al. 2022a, b). Therefore, it is important to investigate the impacts of these influencing factors on meteorological and agricultural extreme drought events (Park et al. 2018; Singh et al. 2022a, b; Williams et al. 2020). The impacts of global warming are manifested through an increase in the frequency and intensity of extreme meteorological and AD events, causing enormous socioeconomic and ecological losses (Asadi Zarch et al. 2015; Dai 2013; Gu et al. 2020; Zhao et al. 2017). Zhang et al. (2014) found that the Yellow River Basin (YRB) is dominated by precipitation amount deficits, further exacerbating the shortage of water resources. Huang et al. (2015a) highlighted greater drought risks in the YRB in spring and winter than in other seasons. Zhao et al. (2021) indicated higher drought levels in the northwestern part of the YRB than those in the southwestern and southeastern parts from 2003 to 2019. Wang et al. (2022a, b) found that most of the YRB area had undergone progressively drier conditions during the 1956–2016 period. However, there is still a lack of studies on the variations in drought characteristics over extended periods and different subperiods at abrupt climate change points in the YRB. Human activities had significant effects on AD propagation. Indeed, Shi et al. (2022) demonstrated that cropland was less sensitive to drought events in the YRB due to irrigation. Cao et al. (2022) highlighted higher contributions of human activities to AD than those of climatic factors, especially in the Loess Plateau of the YRB. This finding suggests the combined effects of both climate change and human activities on drought characteristics. However, the above-cited studies have only explored the impacts of climate change over different study periods, neglecting the potential impacts of human activities.

In recent years, various drought indices have been developed and extensively employed in several regions worldwide to monitor and assess drought characteristics (Adnan et al. 2017; Dehghannik et al. 2021; Kumar Masanta and Srinivas 2022; Wang et al. 2018). The standardized precipitation

index (SPI) and standardized precipitation evapotranspiration index (SPEI) are the most commonly used MD indices (Thomas B. McKee et al. 1993; Vicente-Serrano et al. 2010). However, the SPI only considers precipitation data, making it challenging to compressively interpret drought conditions induced by global warming. Therefore, the SPEI is the most suitable index to study the potential impacts of climate change on MD. Adnan et al. (2017) compared various drought indices, including the SPI, SPEI, China Z-Index, deciles index, and reconnaissance drought index (RDI), to monitor drought conditions in Pakistan, highlighting the suitability of the SPI, SPEI, and RDI to monitor drought status. Gu et al. (2020) used the SPEI and predicted an increase in magnitude and socioeconomic exposure of global droughts in areas with 1.5 and 2 °C warmer climates. On the other hand, the standardized soil moisture index (SSMI) can reflect the dynamic balance of precipitation, groundwater supplies, and evapotranspiration rates, thus comprehensively monitoring AD. The SSMI is advantageous due to its low computational requirements and ability to consider the characteristics of data function distribution (Maity et al. 2016). Suman and Maity (2021) used the SSMI to investigate the intensity and frequency of future AD across India at the basin scale. Han et al. (2021a, b) used the SSMI to quantify the spatiotemporal dynamics of AD in the Loess Plateau, highlighting frequent AD events in the northwestern part of the Plateau, with short durations and low intensities. Afshar et al. (2022) investigated global spatiotemporal consistency between MD and soil moisture indices using the SPI/SPEI and SSMI, respectively, indicating a good positive correlation between the SPEI and SSMI. Therefore, we selected the SPEI and SSMI to monitor MD and AD, respectively, based on their effectiveness reported in previous related studies.

Drought propagations represent the transformation of hydro-climatic signal anomalies as they move through the interconnected terrestrial parts involved in hydro-meteorological cycles (i.e., soils, surface water, and groundwater) (Van Loon 2015). The combined effect of climate change and human activities can change multiple drought properties, including the timing of different drought stages (e.g., onset, development, and recovery), frequency, duration, and intensity (Zhang et al. 2022). Researchers have mainly focused on drought propagation from meteorological to hydrological drought under the impacts of climate variability and human activities. For instance, Zhao et al. (2014) quantitatively assessed the impacts of climate variability and human activities on streamflow in the middle reaches of the YRB in China. Rangelcroft et al. (2019) proposed an observation-based method to quantify the human activity influence on hydrological droughts. Drought propagation from MD to AD is related to the response of soil moisture (or crop yields) to precipitation and other meteorological variables, playing a key role in ensuring food security

(Behrang Manesh et al. 2019; Dai et al. 2022). In addition to precipitation deficit, increased evapotranspiration rates can further deplete soil moisture, triggering or amplifying AD. Groundwater recharge and irrigation play a significant role in decreasing the intensity of MD, mitigating the occurrence of AD (Fang et al. 2020; Wu et al. 2021). Wang et al. (2021) investigated the effects of climate change and human activities on drought propagation from meteorological to hydrological drought using a natural and human-impacted catchment comparison method. Chen et al. (2019) compared the evolution and properties of meteorological, agricultural, and hydrological droughts, as well as their related driving factors, in the Luanhe River basin in China. However, although they considered the entire time period of whole year based on the grid data, different responses of crop species to MD were neglected, making it difficult to comprehensively reflect actual drought propagation characteristics from MD to AD under different periods of crop growth cycles. The impacts of MD to AD propagation remain uncertain on spring and winter wheat on a regional scale in the YRB.

Therefore, the main objective of this study was to better understand the propagation mechanisms of AD in the YRB for spring and winter wheat during the 1950–2021 period. The specific objectives of this study are to 1) select different degrees of human-impacted catchment areas by combining the analysis results of hydrological variations with human influence scores; 2) quantitatively assess drought characteristics (e.g., drought trends, durations, and intensities) and propagation time using the Spearman rank correlation

coefficient and run theory; and 3) compare drought characteristics and propagation time during different sub-periods to reveal the impacts of climate change and human activities on drought characteristics and propagation.

## Materials and methods

### Study area and data

The YRB is located in a typical arid and semiarid region in North China (32.12° N–41.92° N; 95.85° E–119.10° E), covering an area of 752,443 km<sup>2</sup> (Fig. 1). The average elevation of the basin is 1877 m, with minimum and maximum elevation values of –20 m (eastern estuary of the YRB) and 6250 m, respectively, following a decline from the western to eastern parts. The region is characterized by a temperate monsoon climate, with summer months (June–September) receiving approximately 70% of annual precipitation. The annual evapotranspiration (ET) rate of the YRB is 1100–2500 mm, exceeding that of precipitation (200–1000 mm), with relatively low relative humidity values (Li et al. 2022). In this study, we selected 25 catchments from the YRB (Fig. 1), including 12 upstream catchments from southwest to northeast, 11 midstream catchments, and two downstream catchments. Details on the 25 catchment areas are provided in supplementary S1. The data used in this study mainly consists of remote sensing inversion and reanalysis data (Table 1). The remote sensing data were

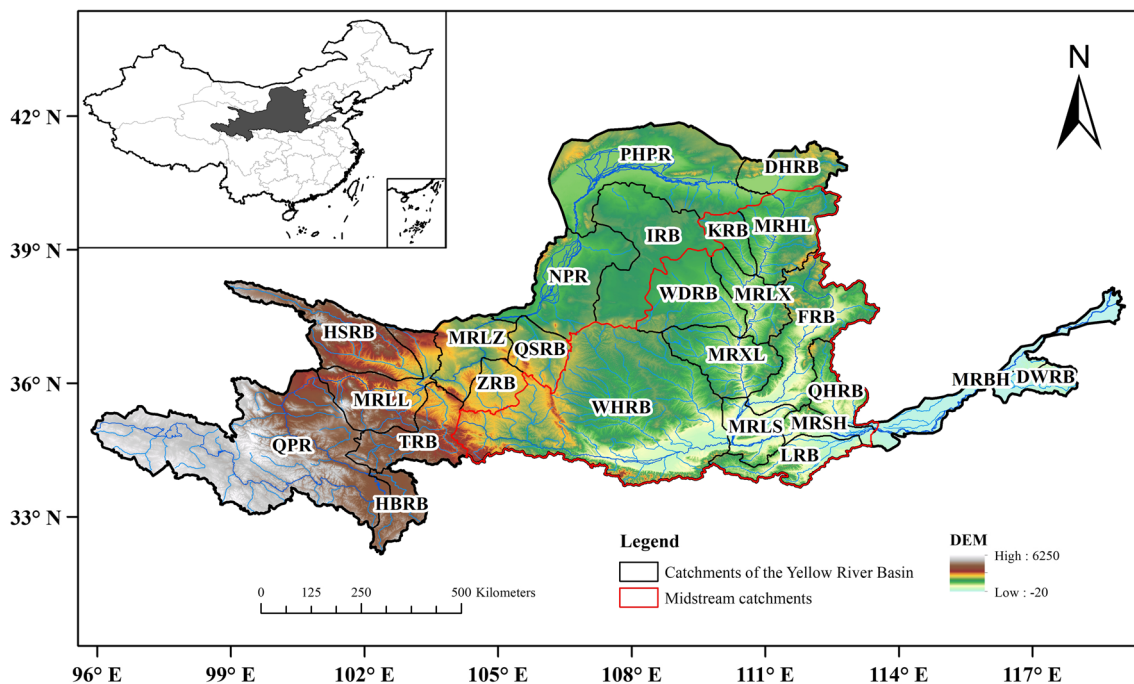


Fig. 1 Location and catchments of the Yellow River Basin. Catchments’ full information is in Supplement S1

**Table 1** Detail information of remote sensing inversion and reanalysis data used in this study

Data types	Temporal coverage	Temporal resolution	Spatial resolution	Units	Data sources
Precipitation	1950–2021	Monthly	0.1°	m	<a href="https://cds.climate.copernicus.eu">https://cds.climate.copernicus.eu</a>
Evaporation	1950–2021	Monthly	0.1°	m	<a href="https://cds.climate.copernicus.eu">https://cds.climate.copernicus.eu</a>
Surface soil moisture	1950–2021	Monthly	0–28 cm, 0.1°	m <sup>3</sup> /m <sup>3</sup>	<a href="https://cds.climate.copernicus.eu">https://cds.climate.copernicus.eu</a>
Digital elevation model (DEM)	2000	-	250 m	m	<a href="https://www.resdc.cn">https://www.resdc.cn</a> , (Xu 2020)
Teleconnection factors	-	Monthly	-	-	<a href="https://psl.noaa.gov">https://psl.noaa.gov</a>
Land use and cover	2010	Yearly	1 km	-	<a href="https://www.resdc.cn">https://www.resdc.cn</a> , (Xu et al. 2018)
GDP density	1995, 2000, 2005, 2010, 2015, 2019	Yearly	1 km	Million RMB/km <sup>2</sup>	<a href="https://www.resdc.cn">https://www.resdc.cn</a> , (Xu 2017a)
Population density	1995, 2000, 2005, 2010, 2015, 2019	Yearly	1 km	Persons/km <sup>2</sup>	<a href="https://www.resdc.cn">https://www.resdc.cn</a> , (Xu 2017b)
Night light density (DMSP-PLS)	1992–2013	yearly	0.008°	DN/km <sup>2</sup>	<a href="https://www.resdc.cn">https://www.resdc.cn</a> , (Xu 2022)
Night light density (NPP-VIIRS)	2012–2021	yearly	0.004°	DN/km <sup>2</sup>	<a href="https://www.resdc.cn">https://www.resdc.cn</a> , (Xu 2022)

interpreted at a spatial resolution of  $0.1^\circ \times 0.1^\circ$  using a bilinear method. The growth periods of winter and spring wheat in the YRB are from October to May of the following year and from March to July, respectively (He et al. 2017; Shao and Yan 2007). Areas where spring and winter wheat are cultivated in the YRB are shown in Fig. 4b. The results in this study were analyzed on cropland pixels in areas where spring and winter wheat are cultivated.

## Methodology

In this study, we used a modified observation-based natural and human-impacted catchment comparison method proposed by Wang et al. (2021) (Fig. 2) to assess the impacts of climate change and human activities on drought characteristics and propagation from MD to AD, according to the following three steps:

### Step 1. Catchment and period classifications

The hydrological regime changes in each catchment were identified using the modified Mann–Kendall (MMK) trend analysis and heuristic change-point segmentation of annual precipitation amounts, ET rates, and annual soil moisture contents in the 1950–2021 period. The final change points were determined by averaging all change points of the selected catchments. The entire study period was also divided into different sub-periods. In addition, four socioeconomic indicators of each catchment, namely average population, gross domestic product (GDP), night light data, and proportions of cropland and urban land, were used to

calculate the human influence score using an indicator-based method. The catchments of the YRB were categorized into different human influence degrees (HId) based on the human influence scores.

### Step 2. Quantitative assessment of the drought propagation characteristics

Run theory was first used in this study to identify SPEI and SSMI-based drought durations and intensities at three timescales of 1, 3, and 12 months, representing monthly, seasonal, and annual drought, respectively, thus adequately depicting the evolution of the drought events. In addition, Spearman rank correlation analysis was used to cross-correlate the SPEI accumulation period of 1–48 months (SPEI- $n$ ,  $n = 1, 2, 3, \dots, 48$  months) and the SSMI-1 time series (1 is 1-month scale). This analysis was performed to determine the most appropriate propagation time from MD to AD based on the strongest correlation of the SPEI accumulation period with SSMI-1.

### Step 3. Assessment of the impacts of different factors on the drought characteristics and propagation

To evaluate the impacts of climate change and human activities on the drought characteristics and propagation, different comparison schemes were designed (Fig. 2). Indeed, the drought characteristics and propagation features were compared under different scenarios (I, II, and III) using analysis of variance with one-way ANOVA. In scenario I, drought characteristics and propagation time of different HId

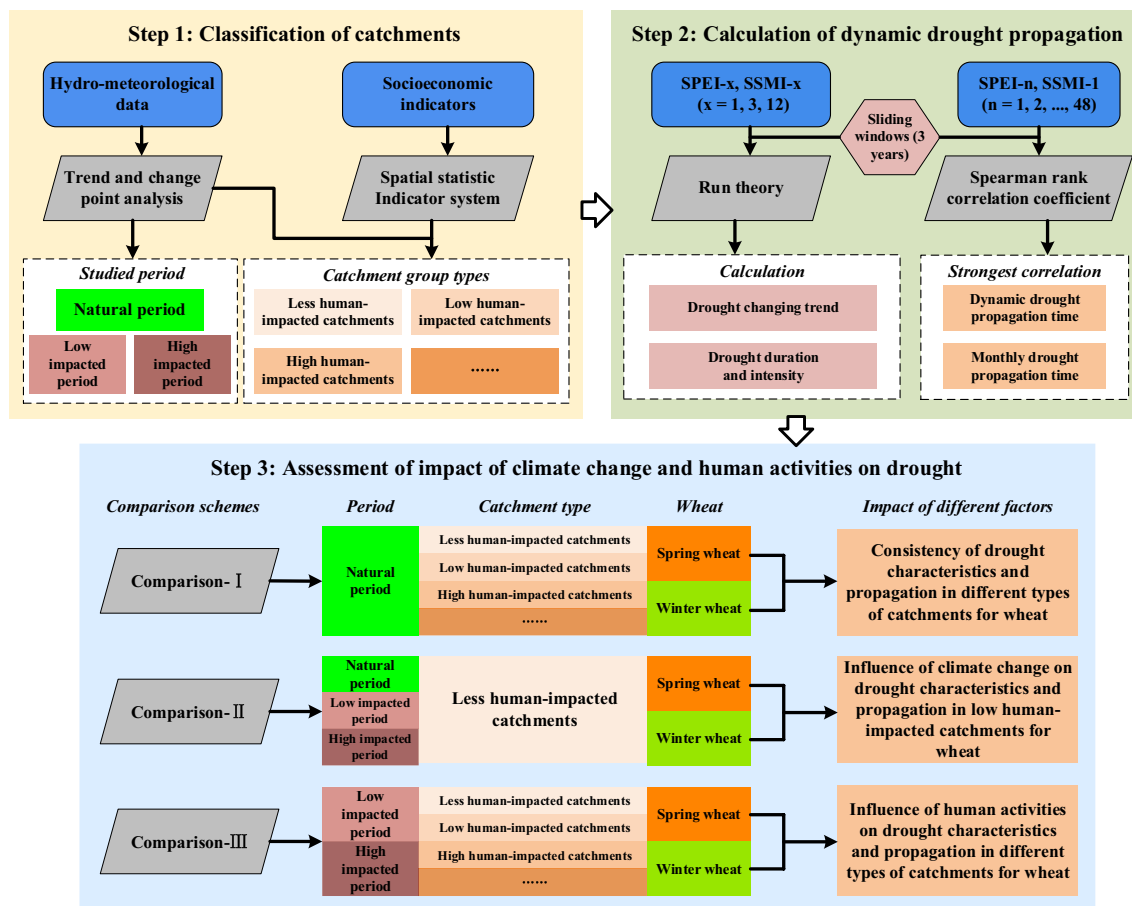


**Fig. 2** An observation-based different human influence strength catchments’ comparison method for analyzing the effects of climate change and human activities on drought characteristics and propagation

catchments were compared to investigate the drought propagation pattern during the natural period (without human activity impacts). In scenario II, the impacts of climate change on the drought characteristics and propagation were assessed in catchments less impacted by human activities during three classified sub-periods of 1950–2021, namely, 1950–1971, 1972–1995, and 1996–2021. In scenario III, the impacts of climate change on the drought characteristics and propagation times were assessed in all catchments over periods with low and high impacts of human activities. The concept underlying this approach and the methods used are described in detail in the following sections.

**Trend and change point analysis**

**Modified Mann–Kendall (MMK) trend analysis**

The MMK trend test was used to assess the statistical significance of SPEI and SSMI-based drought trends. The presence of autocorrelation in the data may result in erroneous results, increasing the probability of detecting trends. Hence, Hamed

and Ramachandra Rao (1998) proposed the MMK trend test to overcome this challenge. The detailed computational processes of the MMK trend test were described in detail by Hamed and Ramachandra Rao (1998).

**Change-point test**

In this study, we determined the change points of hydro-meteorological variable time series using the heuristic segmentation method. This method was first proposed by Bernaola-Galvan et al. (2001) based on the sliding *t*-test, then extensively used to identify change points of nonlinear and non-stationary time series. The principle of this method is to move step-by-step a sliding pointer from left to right along the time series to partition non-stationary time series. Afterward, the average values of the left ( $\mu_1$ ) and right ( $\mu_2$ ) subseries are computed (Huang et al. 2015b). For two Gaussian-distributed random series, the difference between the averages of the two subseries at the 95% statistical significance level can be assessed using Student’s *t*-test according to the following formula:

$$t = \left| \frac{\mu_1 - \mu_2}{S_D} \right| \tag{1}$$

where

$$S_D = \left[ \frac{(N_1 - 1)s_1^2 + (N_2 - 1)s_2^2}{N_1 + N_2 - 2} \right]^{1/2} \left( \frac{1}{N_1} + \frac{1}{N_2} \right)^{1/2} \tag{2}$$

where  $S_D$  denotes the pooled variance;  $s_1$  and  $s_2$  denote the standard deviation values of the two-time series; and  $N_1$  and  $N_2$  are the numbers of observations in the two-time series.

The highest  $t$  value can be regarded as an ideal cut-point threshold value. The corresponding statistical significance  $P(t_{\max})$  can be subsequently determined. Since the time series are not independent and cannot be gained in a closed analytical form,  $P(t_{\max})$  does not conform to the standard Student’s  $t$ -test and can be approximately computed as follows:

$$P(t_{\max}) \approx \left\{ 1 - I_{[v/(v+t_{\max}^2)]}(\delta v, \delta) \right\}^\eta \tag{3}$$

where  $\eta = 4.19 \ln N - 11.54$ , and  $\delta = 0.4$  is obtained from the Monte Carlo simulations;  $N$  denotes the number of the time series to be cut;  $v = N - 2$ , and  $I_x(a, b)$  denotes the incomplete beta function.

The time series cannot be split under a lack of statistically significant difference between the average values ( $P(t_{\max})$  less than the threshold of 0.95). Conversely, the time series can be divided into two segments. On the other hand, under a split time series, the above-described procedures can be iteratively

applied to each new segment until achieving a statistically significant value lower than the threshold or a segment length less than the predefined minimum segment length ( $l_0 \geq 25$ ).

### Establishment of an indicator system for assessing human activity influences

Considering the abovementioned factor datasets, an indicator-based system was built to quantitatively assess the human influences and reveal catchments under the natural period and with increased human activities. In this indicator-based system, we combined the four datasets according to the method described by Sanderson et al. (2002) and Woolmer et al. (2008). We presented each factor dataset as an overlaying grid at a spatial resolution of about 0.1°. In addition, we attributed different scores to the factor datasets to reflect their contributions to human activity influences. The sum of the scores of all indicators was considered as the human influence index (HI). The scoring criteria were based on previous related studies (Table 2). Higher and lower scores indicate greater and lower human activity influences, respectively. The areal average HI scores of the selected catchments were calculated using Eq. 4.

$$HI_k = \sum_{i=1}^N HI_i / N \tag{4}$$

where  $HI_k$  represents the areal average HI score of catchments  $k$  ( $k = 1, 2, 3, \dots, 25$ ),  $HI_i$  denotes the HI score of a grid cell in the catchment, and  $N$  denotes the total number of grids in the catchment.

**Table 2** Classification and the corresponding scores of indicators reflecting human influence

Data set	Grade	Score	Reference
Population density (persons/km <sup>2</sup> )	0–167	0	(Perkl 2017)
	168–278	1	
	278–390	2	
	390–501	3	
	501–612	4	
	> 612	5	
GDP density (ten thousand RMB/km <sup>2</sup> )	0–300	1	(Han et al. 2012)
	300–2000	2	
	2000–5000	3	
	5000–10,000	4	
	> 10,000	5	
Night light density (DMSP-OLS; DN/km <sup>2</sup> )	0–12	0	(Ma et al. 2012; Small et al. 2011)
	> 12	1	
Night light density (NPP-VIIRS; DN/km <sup>2</sup> )	0–0.5728	0	(Dong et al. 2020)
	> 0.5728	1	
Land cover	Cropland	3	(Perkl 2017; Theobald 2010)
	Urban land	4	
	Others	0	

## Drought calculation

### Standardized drought index

In this study, we used the SPEI and SSMI to detect the MD and AD, respectively, in the study area. The SPEI values were calculated using the precipitation and evapotranspiration data on multi-time scales, while the SSMI values were determined using the soil moisture content data on a monthly scale. In addition, water deficits between the precipitation amounts and evapotranspiration rates were calculated at different time scales (1–48 months). The log-logistic probability distribution was used for the SPEI- $n$  ( $n$  is timescales, month) and SSMI calculations (Vicente-Serrano et al. 2010) after examining several other distributions (e.g., beta, gamma, normal, and exponential).

### Run theory

Run theory was used to recognize the drought event periods (Yevjevich 1967), corresponding to those with continuously lower drought index values (DIV) than a certain threshold. In this study, the DIVs were calculated using SPEI and SSMI values on a monthly scale. Considering the monthly or seasonal patterns of drought indices, the percentile thresholds calculated from the DIVs at corresponding scales were used in this study, namely, 50th ( $R_0$ ), 30th ( $R_1$ ), and 15th ( $R_2$ ) (Xie and Tian 2011; Zhou et al. 2014). The drought event durations and intensities were defined as cumulative periods and the sum of DIVs less than  $R_1$ , respectively, during a drought event. The run theory-based drought identification process was conducted based on the following criteria:

- 1)  $DIV(1 \text{ month}) < R_1$  indicates a drought month;
- 2)  $DIV(\geq \text{consecutive } 2 \text{ months}) < R_1$  indicates months with a single drought event;  $DIV(\text{between two consecutive drought events}) > R_0$  indicates two single and consecutive drought events;  $R_1 < DIV(\text{between two consecutive drought events}) < R_0$  indicates two consecutive and combined drought events, with an interval was less than 6 months.
- 3)  $R_2 < DIV(1 \text{ month}) < R_1$  indicate an excluded month from the drought event duration. Otherwise, the month represents a single drought event duration, with a one-month drought event if the DIV is less than  $R_2$ .

## Correlation analysis

### Spearman rank correlation coefficient

Spearman rank correlation coefficient (SCC) was used in this study to assess the relationship between MD (SPEI) and AD (SSMI) (Spearman 2010; Xu et al. 2021). SPEI- $n$

with the strongest SCC with SSMI-1 was regarded as an indicator of the drought propagation period (Huang et al. 2021; Wu et al. 2021; Zhang et al. 2021). A SPEI time scale with the highest SPEI-SSMI correlation coefficient indicates responses of AD to MD. This suggestion is, in fact, based on the notion that the development (i.e., the onset, peak severity, and end stages) of AD is continuously responsive to the persistence of MD events instead of a specific drought stage of previous MD. Hence, the defined AD drought response times in this study highlight the cumulative effects of MD (Fang et al. 2020).

### Cross-wavelet analysis

Cross-wavelet analysis (Grinsted et al. 2004) was used in this study to analyze the relationships between drought propagation (evapotranspiration, precipitation, and soil moisture time series) and teleconnection factors (Niño 4 SST index, Southern Oscillation Index, and Sunspot Index). This method can effectively assess the correlation between two-time series in a time–frequency domain. The detailed computational processes of cross-wavelet analysis were described by Grinsted et al. (2004) and Tian et al. (2022).

## Results

### Classifications of the catchments and study period

The MMK results of all catchments generally showed a decreasing trend of SPEI and SSMI during 1950–2021 at the significant level ( $\alpha=0.05$ ) (Table 3). All catchments with significant decreasing trends of precipitation ( $P$ ), evapotranspiration (ET), and soil moisture (SM) time series showed heuristic segmentation-based change points in 1969/2004, 1970/1995, and 1971/1997, respectively (Table 3). On the other hand, no significant trends were observed in the TRB, QPR, MRL, and HSRB catchments, with a lack of change points for  $P$  and SM. The entire study period was classified into three sub-periods for further analysis according to the above-described results, which are the natural period (without human activity impacts) (NP), the period with low human activity impacts (LP), and the period with high human activity impacts (HP), corresponding to 1950–1971, 1972–1995, and 1996–2021, respectively.

According to the temporal variation in the cropland and urban land proportions (Fig. 3a), all catchments showed increasing trends, except for the QHRB, MRL, MRXL, WHRB, WDRB, MRLX, and MRHL catchments. The average GDP density exhibited an increasing trend throughout all catchments, especially in the MRBH, DWRB, MRSH, and LRB catchments (Fig. 3b). The average population density (Fig. 3c) also displayed an increasing trend during the

**Table 3** Results of the modified Mann–Kendall (MMK) trend analysis and change point tests of annual precipitation (*P*), annual evapotranspiration (ET), and annual accumulated soil moisture (SM) for catchments

Catchment	MMK trend			Heuristic segmentation for the change point		
	<i>P</i>	ET	SM	<i>P</i>	ET	SM
HBRB	2.09↑*	−3.02↓*	2.43↑*	1988*, 1956*	1975**, 2001*	1979**
LRB	−3.42↓*	−1.56↓	−4.93↓*	1965**, 2006*	2010**	2006**
MRSB	−4.31↓*	−2.91↓*	−5.57↓*	1964**, 2005*	2007**	2006**
MRLS	−3.62↓*	−4.16↓*	−5.24↓*	1964**, 2004*	2007**	2005**, 1964*
TRB	−0.59↓	−0.17↓	−1.63↓	-	-	-
QPR	2.89↑*	−1.13↓	1.24↑	1987*, 1955**	1956**	1956*, 1985**
ZRB	−1.05↓	0.27↑	−2.13↓*	-	-	1971*
DWRB	−2.20↓*	−2.30↓*	−3.56↓*	1964*	2010*	1964**
QHRB	−5.05↓*	−3.99↓*	−6.18↓*	1977**, 2004*	2007**	2005**, 1964*
MRLI	−1.13↓	−0.70↓	−2.56↓*	-	1959*	-
MRXL	−4.46↓*	−4.25↓*	−5.88↓*	1969**	1995**	1995**, 1964*
WHRB	−3.17↓*	−1.99↓*	−4.14↓*	1965**	2007*	1997**
QSRB	−1.99↓*	−2.08↓*	−3.15↓*	-	-	1971**
MRLZ	−1.33↓	−1.66↓	−2.86↓*	-	-	1971**
HSRB	−0.56↓	0.37↑	−2.28↓*	-	1965*, 1996**	-
MRBH	−2.99↓*	−3.83↓*	−4.53↓*	1965**	2009**	1965**, 2006*
WDRB	−3.87↓*	−3.59↓*	−4.63↓*	1969**	1970**	1970**
MRLX	−4.47↓*	−4.13↓*	−5.67↓*	1969**	1970**	1970**, 1997**
FRB	−5.16↓*	−5.59↓*	−6.40↓*	1969**	1992**	1996**, 1964*
NPR	−2.06↓*	−2.44↓*	−3.11↓*	1969*	1970*	1970**
KRB	−2.85↓*	−3.12↓*	−4.37↓*	1969**	1964**	1970**
IRB	−2.20↓*	−2.16↓*	−3.36↓*	1969*	1970*	1970**
MRHL	−4.21↓*	−3.69↓*	−5.10↓*	1969**	1964**	1997**, 1970*
DHRB	−3.58↓*	−3.34↓*	−4.96↓*	2004**	2005**	2005**
PHPR	−1.79↓	−1.96↓*	−3.15↓*	-	-	1980*

“↑” is the increasing trend; “↓” is the decreasing trend

\*  $p < 0.05$

\*\*  $p < 0.01$

1990–2021 period, particularly in the MRBH, FRB, MRLS, DHRB, and MRLZ catchments. The night light density (Fig. 3d, e) also displayed an increasing trend in all catchments, especially in the MRBH, DWRB, and FRB catchments. The human influence score (Fig. 3f), calculated using the abovementioned four indicators (“Impacts of climate change and human activities on the drought propagation”), showed sharp increases in all catchment areas, except for ZRB, MRLI, TRB, QPR, and HBRB. The spatial distribution of the socioeconomic indicators, land use data, and human influence scores of the YRB in 2010 was analyzed (Supplement S1), showing similar spatial patterns. In general, all these indicators showed obvious increasing trends in the upstream, midstream, and downstream catchments of the study area.

The YRB catchments were classified into five human activity influence degrees based on the obtained human influence score results over the 1995–2015 period (Fig. 4a), namely, HI-I, HI-II, HI-III, HI-IV, and HI-V, to reflect the potential human activity impacts on drought propagation.

The results revealed spatial differences in the human activity influence classes. Indeed, HI-I (HBRB, TRB, QPR, MRLI, HSRB, and IRB catchments), HI-II (ZRB, MRXL, QSRB, MRLZ, WDRB, MRLX, NPR, KRB, MRHL, and PHPR catchments), HI-III (QHRB, WHRB, FRB, and DHRB catchments), HI-IV (LRB, MRSB, and MRLS catchments), and HI-V (DWRB and MRBH catchments) had average HI ranges of  $\leq 1.7$ , 1.7–2, 2–3, and 3–4, respectively. The spatial HI scores under the wheat genotypes and dryland areas (from land use data) in the YRB are shown in Fig. 4b.

## Drought characteristics of the meteorological and agricultural droughts

### Evolution of the meteorological and agricultural drought characteristics

In this study, spring and winter wheat displayed insignificant SPEI-1- and SPEI-3-based MD trends in all HI classes in the study period, except in June and May for



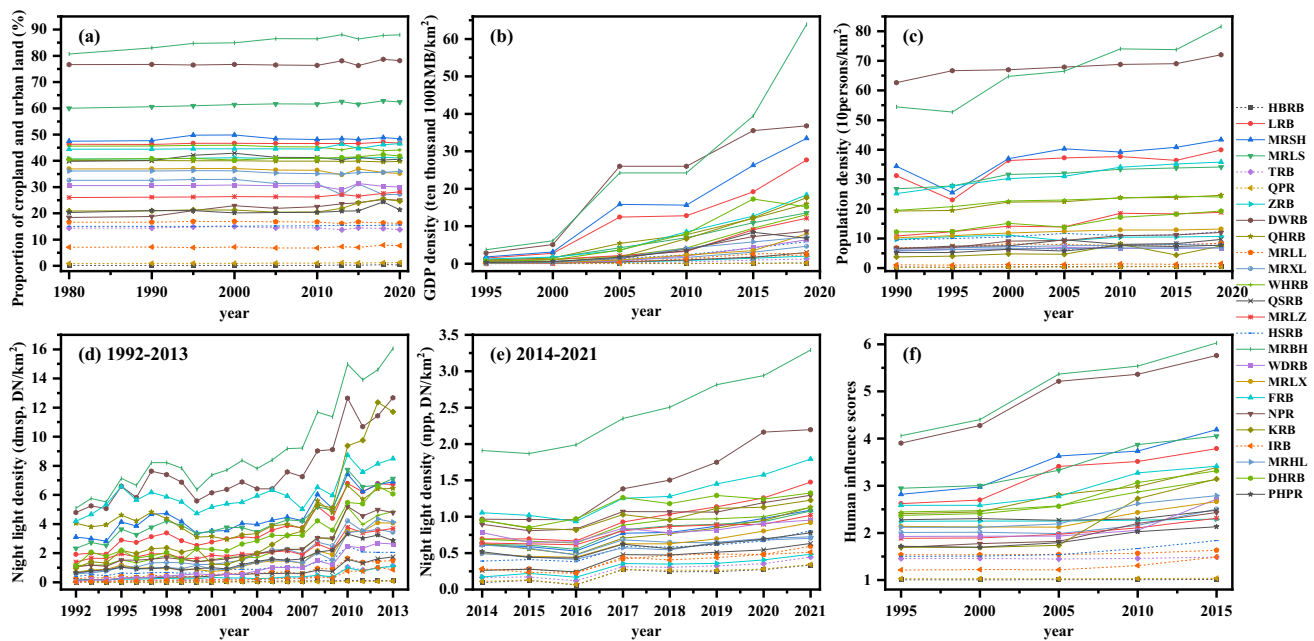


**Fig. 3** Temporal changes of proportion of cropland and urban land (a), average GDP density (b), population density (c), and night light density (d, e), and human influence scores (f) for each catchment in the Yellow River Basin

spring wheat and March, April, and May for winter wheat (Fig. 5a, b, d, e). This finding is consistent with those revealed by (L. Han et al. (2021a, b) and F. Wang et al. (2022a, b). Spring wheat in the Hid-III class area and winter wheat in the Hid-II, III, and IV class areas of SPEI-3 showed significant drying trends (Fig. 5c, f). The MD trend values for winter wheat were relatively higher than those for spring wheat, demonstrating the stronger drying trend of winter wheat. This finding might be due to the differences in the climatic conditions between the spring and winter wheat regions (Gevaert et al. 2018; Xu et al. 2021). On the other hand, both spring and winter wheat displayed a significant AD-based drying trend at all time scales (SSMI-1, SSMI-3, and SSMI-12 time series) in almost all Hid classes. Indeed, Guo et al. (2023) also found similar AD characteristics. In addition, the AD trend for winter wheat is likely to be worse than that for spring wheat (Fig. 5), which is consistent with the results revealed by Wang et al. (2017). This finding suggests strong human activity impacts on AD for winter wheat. It was found that different intensities of human activities had significant influences on the AD for winter wheat. Overall, the SPEI-based drying trend was weaker than that of the SSMI in all Hids, suggesting the occurrence of an AD with a severe magnitude in the YRB. The SPEI and SSMI-based drying trends for spring wheat were obviously weaker than those for winter wheat in almost all Hids, indicating that spring wheat might experience slighter MD and AD as compared with winter wheat during the 1950–2021 period. These

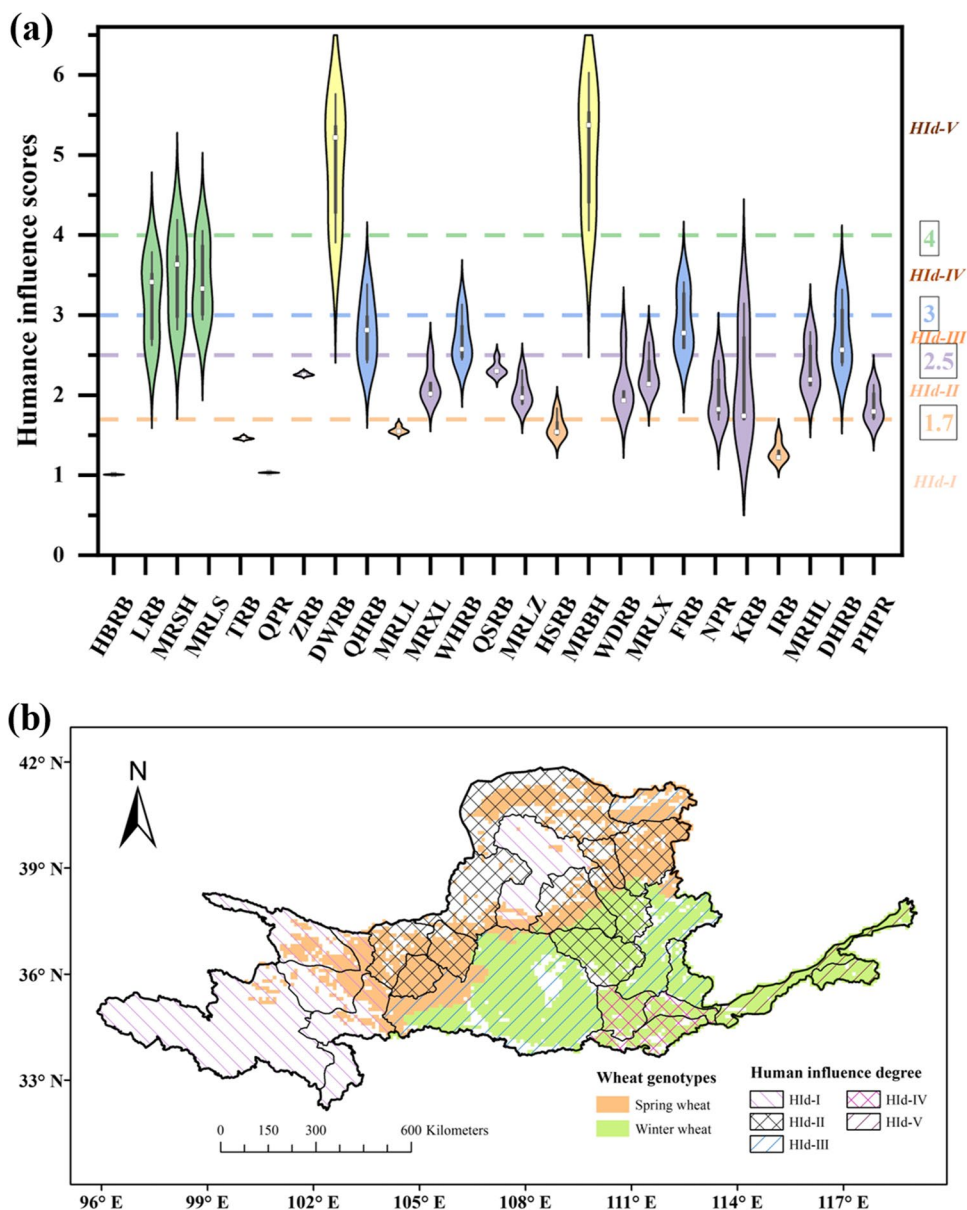
findings are in line with the spatiotemporal dynamics of MD and AD revealed by Han et al. (2021a, b).

The meteorological drought intensity (MDI) for spring wheat (Fig. 6a, b) under all Hids showed a weakening trend from NP to LP and HP. On the other hand, the agricultural drought intensity (ADI) showed increasing trends under all Hids from NP to LP and HP, which is consistent with the spatiotemporal variations revealed by Han et al. (2021a, b) and Wang et al. (2017). The differences in the MDI and ADI between the Hids displayed a lack of consistent characteristics under the different sub-periods. The MDI and ADI for winter wheat (Fig. 6b, d) exhibited weakening trends under all Hids. In addition, the relationship between the MDI and ADI under the lowest and highest Hids was relatively stable when compared to those under the other Hids for winter wheat. MDI and ADI under the middle Hids (Hid-III and Hid-VI) showed unstable relationships with other Hids, suggesting the influences of climate change and human activities on MD and AD under the lowest and highest Hid, respectively, as well as the combined influence of climate change and human activities under the middle Hids. These difference patterns are consistent with the results of Ayan-tobo et al. (2017) and Liu et al. (2016).

### Dynamic characteristics of the meteorological and agricultural droughts

According to the obtained results, all Hids showed insignificant SPEI-3-based drying trends ( $p > 0.05$ ), except for Hid-V

**Fig. 4** Violin plot for human influence scores during 1995–2015 (a) and spatial pattern of spring and winter wheat and human influence degree (b) of all catchments in Yellow River Basin. HI-d-I is the lowest degree, and HI-d-V is the highest degree of human influence. White is not spring and winter wheat region



and HI-d-II with winter wheat and spring wheat, respectively (Fig. 7). This finding suggests the occurrence of widespread and increased MDI in the YRB, which is in line with the results of Han et al. (2021a, b). Particularly, a significant drying trend was observed in HI-d-III with spring wheat ( $p < 0.05$ ). Severe MDI values were observed under all HIDs during the NP, followed, respectively, by those observed in the HP and LP for both spring and winter wheat. The lowest average MDI value was observed in the LP, which is consistent with the results shown in Fig. 6. The results showed a similar trend pattern of the MDI under the same HIDs of spring and winter wheat in all sub-periods. More severe MDI was observed for spring wheat, while MDI of HI-d-III were inconsistent with those of other HIDs during the HP, suggesting the influence of human activities on regional

climatic conditions. This finding is, indeed, consistent with the results revealed by Wang et al. (2017). In addition, the MDI indicated an insignificant wetting trend in the HP for both spring and winter wheat under all HIDs, except for HI-d-V, which is in line with the results of Zhao et al. (2023). In general, greater fluctuation and more severe MDI were observed for both spring and winter wheat in areas with the highest HI-d during the 1950–2021 period.

The SSMI-3-based dynamic ADI (Fig. 8) showed a significant drying trend ( $p < 0.01$ ) showing a higher changing rate than that of the MDI of SPEI-3. Both MDI and ADI displayed a stronger decreasing trend during the LP than that in the NP. In addition, an increased drought intensity was observed in the HP than that in the LP, which is consistent with the finding found by Wang et al. (2017). Unlike MDI,

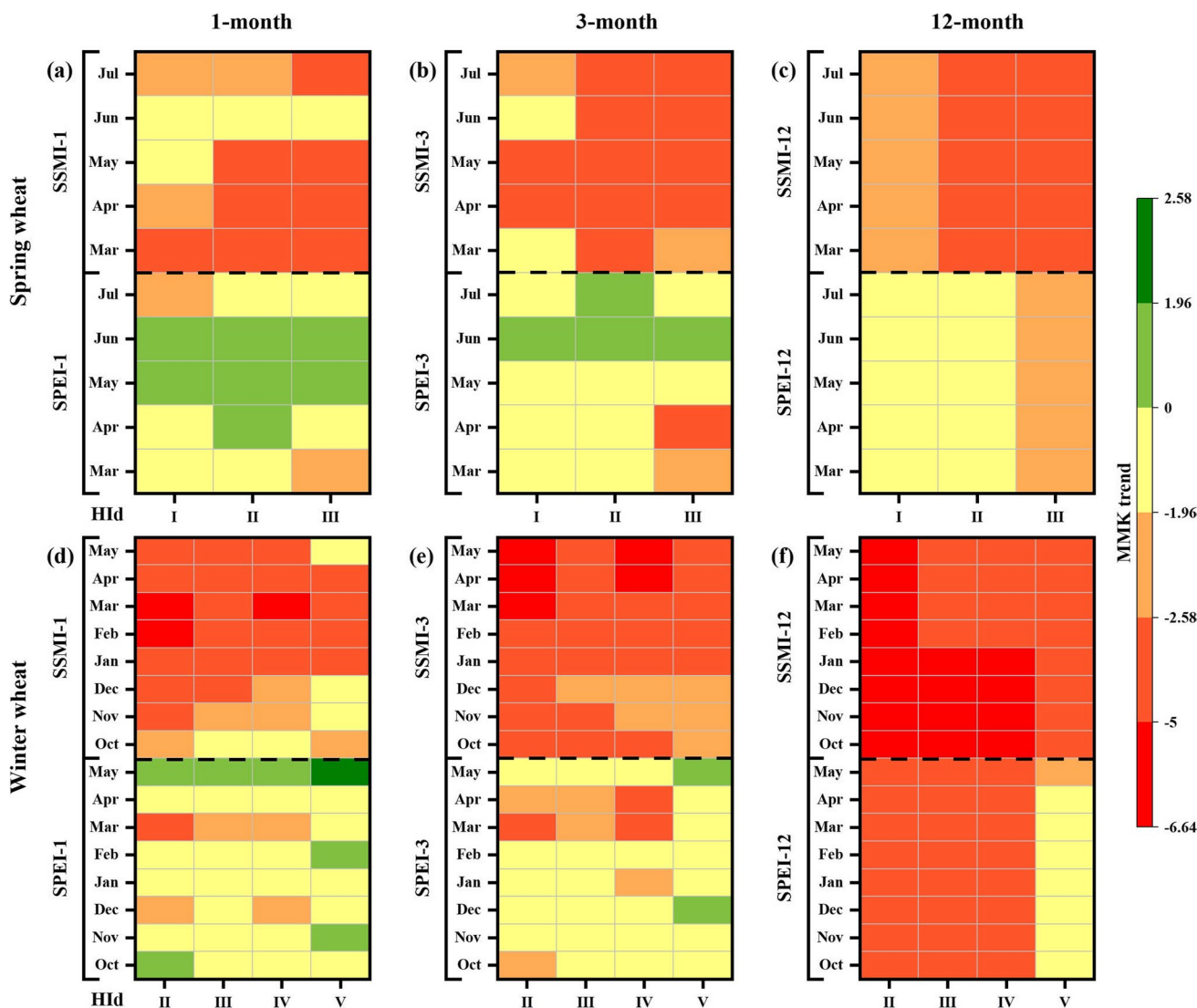


**Fig. 5** Monthly modified Mann–Kendall (MMK) trends in the long-term Standardized Precipitation Evapotranspiration Index (SPEI) and Standardized Soil Moisture Index (SSMI) time series measured at 1-, 3-, and 12-month time scales in the winter and spring wheat grids

for different intensities of human-impacted catchments of the Yellow River Basin from 1950 to 2021. Hid-I is the lowest degree for human influence, and so on. The color bar denotes the value of the Z statistic

obvious differences in the ADI were observed between the three periods, with more severe ADI during the HP compared with those in the other periods. The results showed a severe ADI for winter wheat, with higher linear changing rates, compared to that for spring wheat, indicating the occurrence of more severe AD for winter wheat in the YRB, as shown in Fig. 6. Under the same HIDs, winter wheat had experienced severe ADI and larger changing slopes of dynamic ADI when compared with spring wheat. In addition, larger fluctuation and higher changing rates of the ADI were observed during the HP period from low to high Hid and for both spring and winter wheat, indicating high vulnerability levels of catchments with higher Hid to agricultural drought. Consistent increasing trends of ADI were observed

for both spring and winter wheat in the different sub-periods, demonstrating significant influences of climate change and human activities on agricultural drought. However, a strong influence of human activities was observed on the ADI, particularly in the HP.

**Propagation from meteorological to agricultural drought**

**Temporal evolution of propagation time from meteorological to agricultural drought**

The results showed a temporal change in the drought propagation from 0 and 20 months in all periods and for both

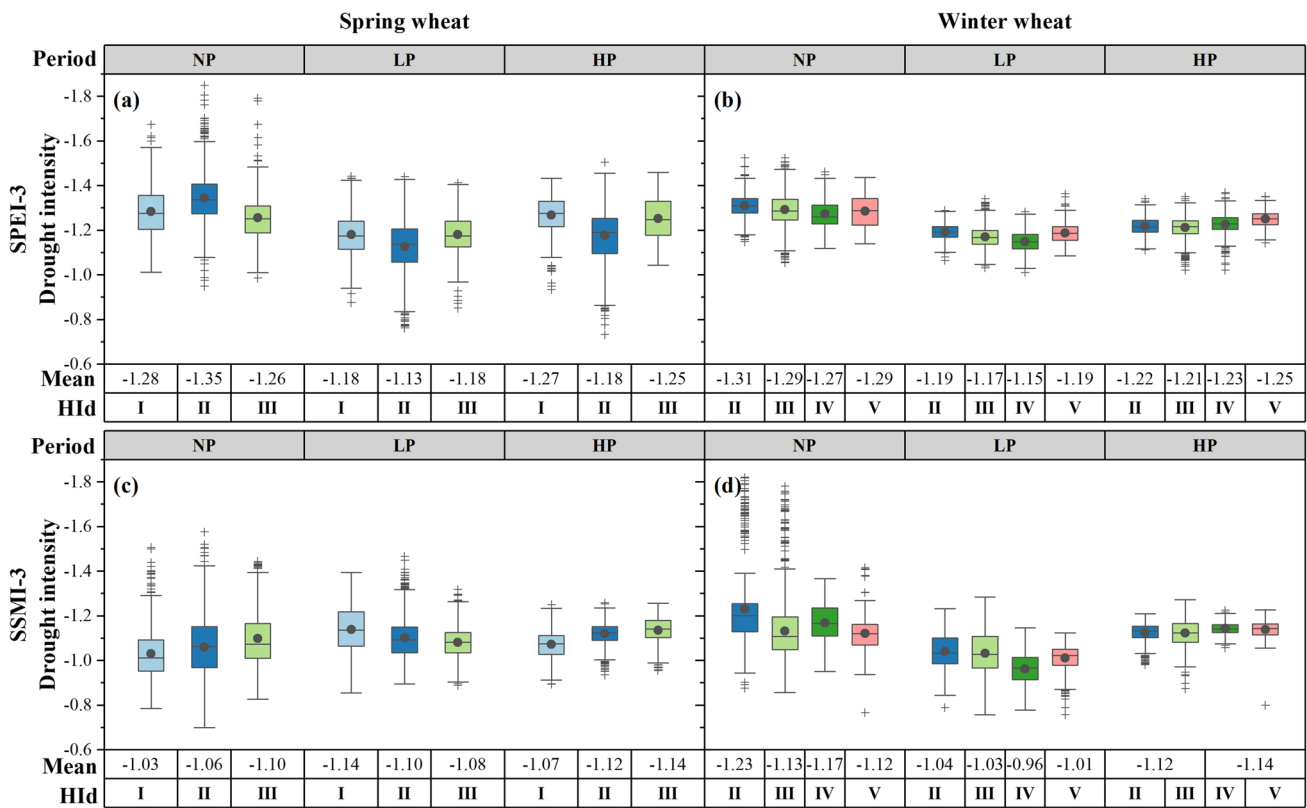


**Fig. 6** Box plots of drought intensity for meteorological and agricultural drought of the catchments of planting wheats in the Yellow River Basin during the natural period without impact of human activities (NP, 1950–1971), the period with low impact of human activities (LP, 1972–1995), and the period with high impact of human activities (HP, 1996–2021), based on the Standardized Precipitation Evapotran-

spiration Index (SPEI) and Standardized Soil Moisture Index (SSMI) time series measured at 3-month time scales. HId-I is the lowest degree for human influence, and so on. The numbers within the figure are the average drought intensity of meteorological and agricultural drought for catchments

spring and winter wheat, of which spring wheat showed a longer propagation time (Fig. 9). This finding is inconsistent with that revealed by Sun et al. (2023), showing an AD propagation time range of 3–12 months. Sun et al. (2023) limited the SPEI to 1–12 month scales and found a longer AD propagation time in spring wheat areas than in winter wheat areas. This was also consistent with the results of F. Wang et al. (2022a, b) and Dai et al. (2022). The inconsistent propagation time results were observed in this study mainly in spring wheat areas under all HIDs. Overall, spring wheat also displayed high drought propagation fluctuations in the HP, suggesting uncertain climate change impacts on drought propagations in the spring wheat areas. Small and high propagation time ranges were observed in the winter and spring wheat areas, respectively. Prolonged drought propagation times were observed in both spring and winter wheat areas under all HIDs during the NP followed by those in the LP and HP. The drought propagation time in the HP period showed prolonged and shortened trends from low to high HIDs in the spring and winter wheat areas, respectively. However, these trends were insignificant during the

LP, indicating a reduced drought propagation time under the influences of climate change and human activities. Dai et al. (2022) also found similar variation patterns of AD propagation time in areas with winter wheat cultivations.

On the other hand, a shortened drought propagation time under HId-I and prolonged propagation times under HId-II and HId-III were observed for spring wheat (Fig. 10). These findings are consistent with those revealed by Zhang et al. (2021). Prolonged drought propagation times for winter wheat were observed during the critical crop growth periods of April and May, as well as for spring wheat in June and July. This finding demonstrates the positive influence of human activities on soil moisture contents at the critical crop growth stages. The drought propagation time was longer in May for both spring and winter wheat in the HP. In fact, this month represents the heading and maturity stages of spring wheat and winter wheat, respectively. The drought propagation time under HId-II was longer than those under other HIDs for both spring and winter wheat. Spring wheat had a longer drought propagation time than winter wheat under HId-II and HId-III. The longest drought propagation times

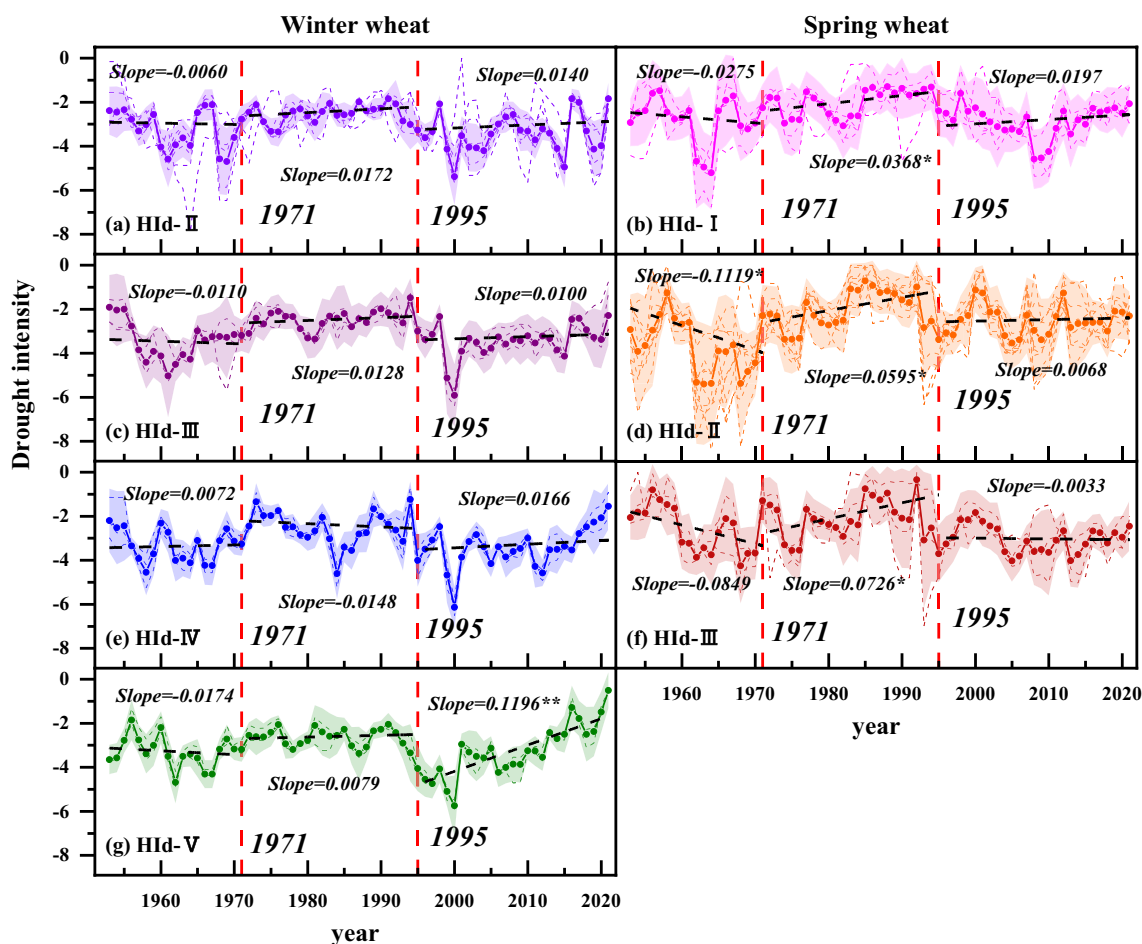


**Fig. 7** Dynamic meteorological drought intensity calculated by the Standardized Precipitation Evapotranspiration Index on 3-month scale (SPEI-3) with 3-year sliding window for spring and winter

wheat of growth period at different intensities of human-impacted catchments. HId-I is the lowest degree for human influence, and so on

were observed in the January–April and March–May periods for winter wheat and spring wheat, respectively.

**Dynamic propagation time from meteorological to agricultural drought**

Overall, only three HIds (HId-II and HId-V for winter wheat and HId-I for spring wheat) showed insignificant drought prolongation trends (Fig. 11) in the YRB. These findings are in line with those revealed by Dai et al. (2022) and Zhang et al. (2021). The longest drought propagation time was observed in the HP under all HIds, followed, respectively, by those in the LP and NP, which is consistent with the results shown in Fig. 9. A prolonged trend of the drought propagation time was observed in areas with winter wheat cultivation under all HIds in the NP. The changing trends of the drought propagation time were consistent with the slope features of the study area. Indeed, decreasing, increasing, and increasing trends were

observed from the lowest to the highest HIds in the NP, LP, and HP, respectively. Significantly prolonged drought propagation trends under high changing slopes and HIds (III–V) were observed in the HP. Similarly to spring wheat, insignificant differences of propagation time were observed in areas with winter wheat cultivation, while significantly prolonged drought propagation trends were observed under high HIds in the HP. The drought propagation time under HId-II and HId-III exhibited similar changing trends for both spring and winter wheat, while a higher changing trend slope and larger fluctuation for winter wheat than those for spring wheat were observed during all sub-periods. The agricultural propagation time differences between crops were also investigated by Shi et al. (2022), highlighting the significant effects of various vegetation types on AD propagation. The drought propagation time showed a significant prolonged and strengthened trend with increasing HId in areas with spring and winter wheat cultivations.

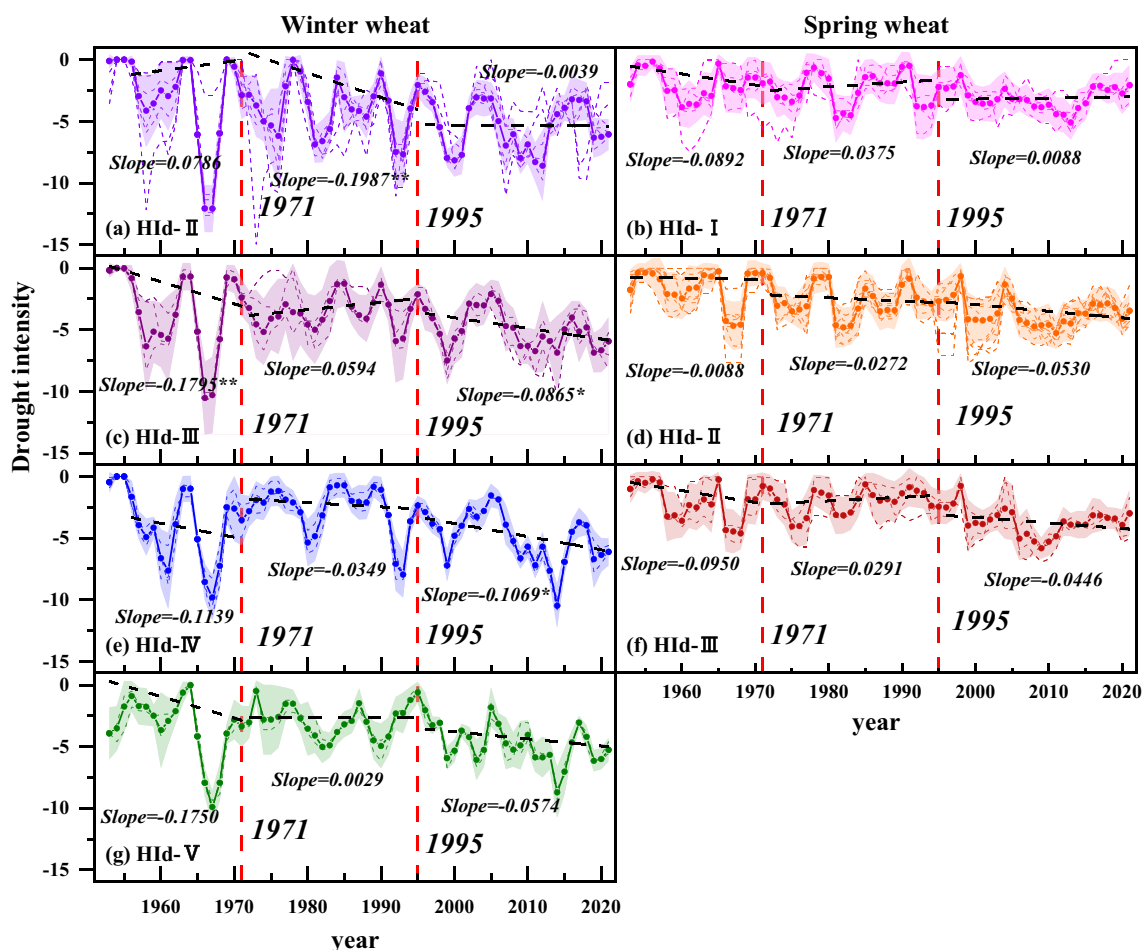


**Fig. 8** Dynamic agricultural drought intensity calculated by the Standardized Soil Moisture Index on 3-month scale (SSMI-3) with 3-year sliding window for spring and winter wheat of growth period

at different intensities of human-impacted catchments. HId-I is the lowest degree for human influence, and so on

### Impacts of climate change and human activities on the drought propagation

In this study, we analyzed the drought characteristics and propagation time during different periods and under different human influence degrees for spring and winter wheat. However, the obtained results did not give statistical tests for the three scenarios (Fig. 2). Therefore, further statistical tests were performed. We compared the drought characteristics and propagation time under different HIDs during the NP (scenario I) (Table 4). Overall, the results of all drought characteristics and propagation time had no significant differences between the different HIDs, except for the MDI and ADI of areas with spring wheat and winter wheat cultivations, respectively. This finding demonstrates the consistency of different HIDs of the YRB catchments for the drought characteristics and the drought propagation times in the NP (without significant influences of human activities), whereas the variance results showed that crop species had

significant influences on the MD and AD drought durations, which might be due to the variations in climatic characteristics and crop growth stages. In addition, the HIDs had significant influences on the AD duration, which might be due to the higher HId drought tolerance. The crop species and HId interactions showed significant influence on the MD duration and MDI due to the impacts of climatic characteristics. In this study, higher MDI values were observed than those of ADI. In addition, shorter MD durations than those of the AD were found in areas with spring and winter wheat cultivations under all HIDs. The drought propagation time was generally less than 10 months for spring and winter wheat and under all HIDs. However, spring wheat had longer drought propagation times than winter wheat under HId-II and HId-III.

The drought characteristics and propagation times in the different sub-periods were compared under HId-I and HId-II for spring wheat and winter wheat, respectively (scenario II) (Table 5). Overall, the drought characteristic

**Fig. 9** Box plots of drought propagation time from meteorological to agricultural drought of different intensities of human-impacted catchments in the Yellow River Basin during the natural period without impact of human activities (NP, 1950–1971), the period with low impact of human activities (LP, 1972–1995), and the period with high impact of human activities (HP, 1996–2021), based on the Standardized Precipitation Evapotranspiration Index (SPEI) and Standardized Soil Moisture Index (SSMI) time series. HId-I is the lowest degree for human influence, and so on. The numbers within the figure are the average propagation time for catchments

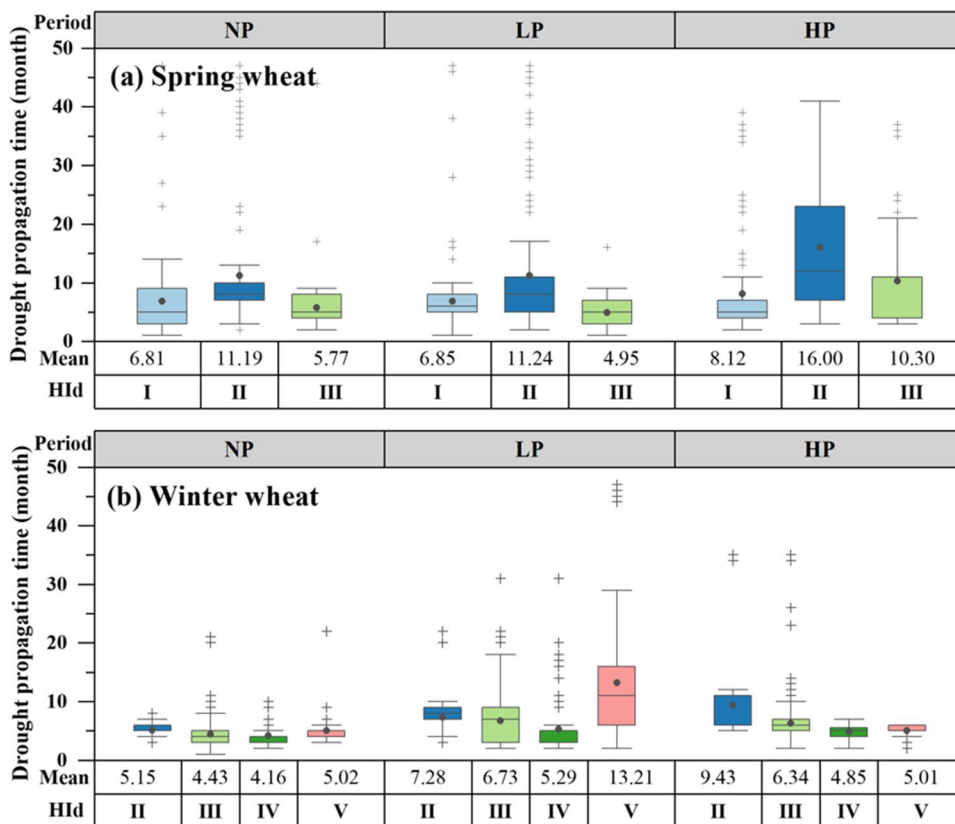
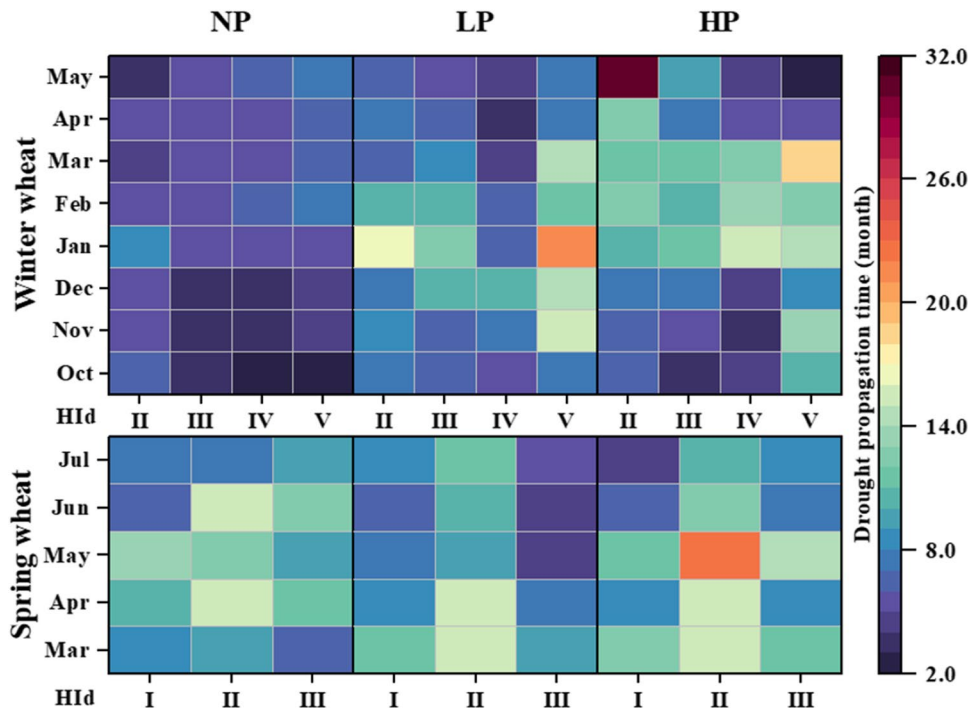


**Fig. 10** Heatmap of drought propagation time from meteorological to agricultural drought of spring and winter wheat at growth months for different intensity of human-impacted catchments during the natural period without impact of human activities (NP, 1950–1971), the period with low impact of human activities (LP, 1972–1995), and the period with high impact of human activities (HP, 1996–2021). HId-I is the lowest degree for human influence, and so on



and propagation time results were significantly different between the sub-periods. This finding suggests significant influences of climate change on the drought characteristics

and propagation times in the different periods for both spring and winter wheat. The observed MDI under HId-I in areas with spring wheat cultivations exhibited

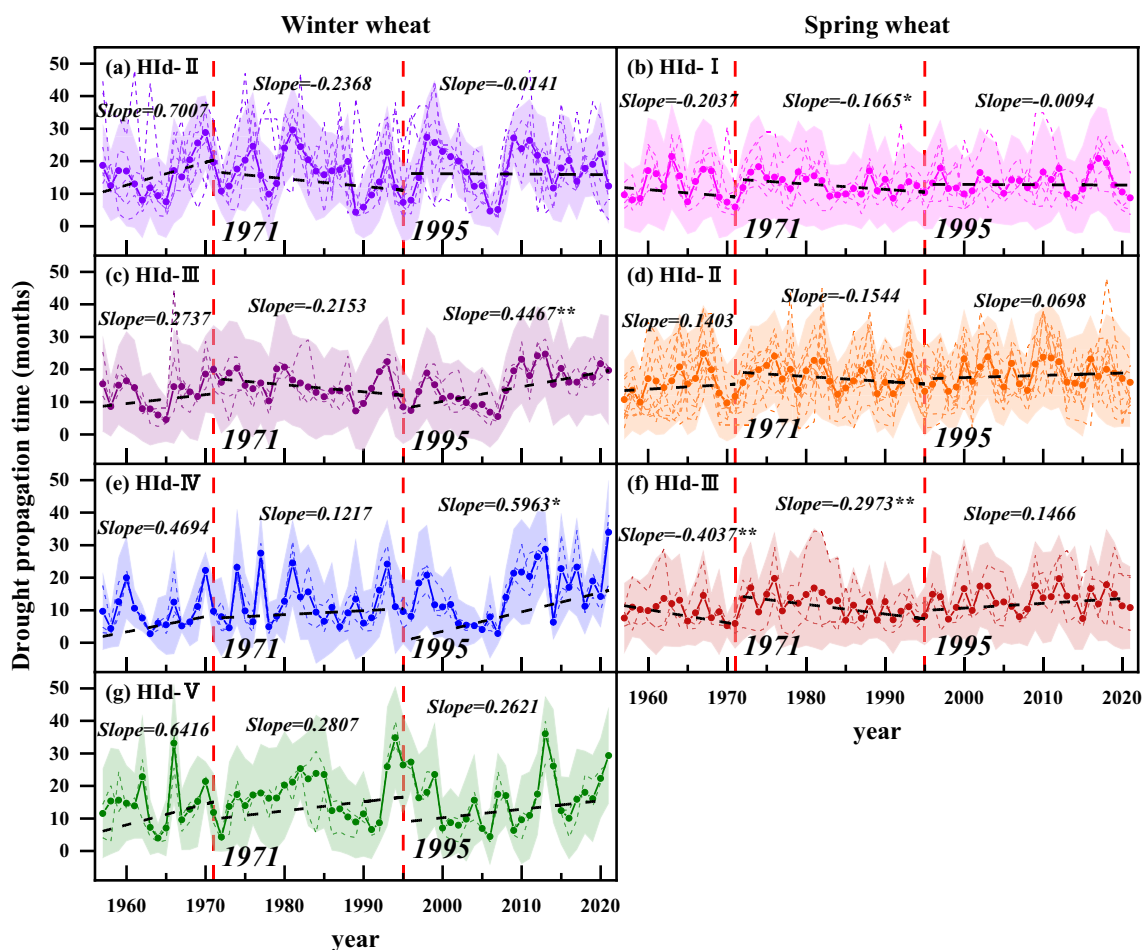


**Fig. 11** Dynamic drought propagation from meteorological to agricultural drought for different intensity of human-impacted catchments for spring and winter wheat in the Yellow River Basin. HId-I is the lowest degree for human influence, and so on

**Table 4** Drought characteristics of meteorological and agricultural droughts and propagation time from meteorological to agricultural drought under different human influenced degrees (HId) under natural period (1950–1971). I is the lowest HId, and V is the highest HId

Crop	HId	Meteorological drought		Agricultural drought		Drought propagation Time (month)
		Duration (month)	Intensity	Duration (month)	Intensity	
Spring wheat	I	2.3 ± 0.19a	-1.29 ± 0.07ab	3.19 ± 0.42a	-1.07 ± 0.13a	8.22 ± 4.36a
	II	2.52 ± 0.37a	-1.36 ± 0.06b	3.15 ± 0.26a	-1.04 ± 0.09a	9.24 ± 4.44a
	III	2.18 ± 0.05a	-1.26 ± 0.01a	3.31 ± 0.25a	-1.09 ± 0.09a	5.61 ± 2.08a
Winter wheat	II	2.52 ± 0.14b	-1.29 ± 0.04a	5.18 ± 0.34a	-1.20 ± 0.14a	5.86 ± 1.14a
	III	2.77 ± 0.17a	-1.30 ± 0.03a	4.92 ± 0.06a	-1.13 ± 0.06a	4.67 ± 0.74ab
	IV	2.76 ± 0.14a	-1.27 ± 0.02a	4.94 ± 0.06a	-1.17 ± 0.05a	4.08 ± 0.54b
	V	2.70 ± 0.13ab	-1.26 ± 0.08a	4.20 ± 0.19b	-1.13 ± 0.01a	4.68 ± 1.03ab
Analysis of variance (F value)	Crop (C)	6.20*	0.24	168.81**	3.66	1.84
	HId (H)	0.17	1.71	3.58*	0.08	0.72
	C × H	5.87*	4.27*	2.19	1.41	0.59

weakening-strengthening trends from the NP to the LP and HP. A similar finding was observed for the MDI and ADI under HId-II in areas with winter wheat cultivations.

On the other hand, the observed ADI in areas with spring wheat cultivation and HId-I showed a stronger strengthening-weakening trend in the NP than those in the LP and



**Table 5** Drought characteristics of meteorological and agricultural droughts and propagation time from meteorological to agricultural drought under different periods for lowest human influenced degrees

(I for spring wheat and II for winter wheat). NP is 1950–1971, LP is 1972–1995, and HP is 1996–2021

Crop	Period	Meteorological drought		Agricultural drought		Drought propagation
		Duration (month)	Intensity	Duration (month)	Intensity	Time (month)
Spring wheat	NP	2.23 ± 0.10b	− 1.29 ± 0.07bc	2.91 ± 0.11b	− 1.01 ± 0.03a	8.22 ± 4.36a
	LP	2.20 ± 0.07bc	− 1.18 ± 0.04a	2.88 ± 0.07bc	− 1.13 ± 0.04b	6.93 ± 2.89a
	HP	2.37 ± 0.10a	− 1.27 ± 0.07b	3.06 ± 0.06a	− 1.06 ± 0.06a	8.55 ± 7.01a
Winter wheat	NP	2.52 ± 0.14b	− 1.29 ± 0.04c	5.18 ± 0.34a	− 1.25 ± 0.05b	5.42 ± 0.51c
	LP	2.36 ± 0.11c	− 1.17 ± 0.04a	5.32 ± 0.46a	− 1.09 ± 0.07a	7.68 ± 0.69b
	HP	2.71 ± 0.12a	− 1.23 ± 0.04b	5.23 ± 0.51a	− 1.11 ± 0.05a	10.67 ± 2.06a

HP. The MD and AD durations in areas with spring wheat cultivations and HI-I exhibited a shortening-lengthening trend from the NP to the LP and HP. A similar finding was observed in areas with winter wheat cultivations and HI-II. The AD duration in areas with winter wheat cultivation and HI-II showed a stronger lengthening-shortening trend in the NP than those in the LP and HP. The drought propagation time for spring wheat under HI-I showed a shortening-lengthening trend, while winter wheat under HI-II experienced a prolonged propagation time in the NP followed by those in the LP and HP. This finding highlights the strong positive influence of climate change on prolonging the drought propagation time.

In scenario III, the drought characteristics and its propagation under low (1972–1995) and high (1996–2021) impacted periods were compared under different HIDs (Table 6). Overall, the drought characteristic and propagation time results exhibited significant differences between the low and high impacted periods under all HIDs and for both spring and winter wheat, except for areas with both HI-III and spring wheat cultivations. This result demonstrates the significant influences of human activities on drought characteristics and propagation times. The variance results showed significant influences of crop style on the MD and AD durations, while the sub-periods exhibited significant influences on the drought characteristics. The HI had significant influences on the drought characteristics and propagation times, except on the ADI. In addition, the period and HI interactions exhibited significant influences on the drought characteristics and propagation times, except on the MDI. Indeed, the MDI and ADI were generally strengthened, while the MD and AD durations were prolonged in areas with spring and winter wheat cultivations and under all HIDs from the LP to the HP. The drought propagation time was generally prolonged in areas with spring and winter wheat cultivations and under all HIDs from the LP to the HP, indicating the significant influences of human activities on disturbing and delaying the natural drought propagation process in areas with wheat cultivations in the LP and HP.

## Discussion

### Influences of the teleconnection factors on the propagation of meteorological droughts to agricultural droughts

Regional extreme hydro-climatic events are closely associated with atmospheric circulation anomalies due to abnormal water vapor transport from the ocean. The sea, land surface temperature, and wind speeds interactions can slightly change the atmospheric boundary conditions, causing regional drought events (Asong et al. 2018; Baier et al. 2022; Han et al. 2019). Nguyen et al. (2023) reported that the strongest ENSO events from December to February might subsequently contribute to the development of MD events from March to May, which might further lead to hydrological and AD from April to June over Mekong River Basin. Adolphi et al. (2014) the effects of solar activities on the variations in sea-level pressure, wind velocity, wind direction, and precipitation to some extent in Greenland. Therefore, atmospheric circulation anomalies and solar activities can influence climate change to some extent. In this study, we assessed the effects of the teleconnection factors (Sunspot Index, Southern Oscillation Index, Niño 4 SST index) on the drought propagation time from MD to AD using cross-wavelet analysis. The results of our study indicate that evapotranspiration, precipitation, and soil moisture were the main influencing factors on the drought events significantly prolonging the drought propagation times in areas with spring and winter wheat cultivations in the YRB. According to Figs. 12 and 13, the selected teleconnection factors exhibited effects on the evapotranspiration rates, precipitation amounts, and soil moisture contents in areas with spring and winter wheat cultivations, of which the Sunspot Index had the strongest effect. The distribution of areas with stronger correlation indicates significant variations in the drought characteristics and propagation during the sub-periods. Therefore, it can be concluded that the teleconnection factors indirectly affected the drought propagation to some

**Table 6** Drought characteristics of meteorological and agricultural droughts and propagation time from meteorological to agricultural drought under different periods and different human influenced degrees (HI<sub>d</sub>). NP is 1950–1971, LP is 1972–1995, and HP is 1996–2021. I is the lowest HI<sub>d</sub>, and V is the highest HI<sub>d</sub>

Crop	HI <sub>d</sub>	Period	Meteorological drought		Agricultural drought		Drought propagation Time (month)	
			Duration (month)	Intensity	Duration (month)	Intensity		
Spring wheat	I	LP	2.20 ± 0.07b	-1.18 ± 0.04a	2.88 ± 0.07b	-1.13 ± 0.04b	6.93 ± 2.89a	
		HP	2.37 ± 0.10a	-1.27 ± 0.07b	3.13 ± 0.16a	-1.04 ± 0.04a	8.55 ± 7.01a	
	II	LP	2.35 ± 0.22a	-1.11 ± 0.07a	3.03 ± 0.18b	-1.09 ± 0.03a	8.29 ± 3.32b	
		HP	2.36 ± 0.09a	-1.21 ± 0.05b	3.42 ± 0.29a	-1.13 ± 0.01b	14.77 ± 6.81a	
	III	LP	2.50 ± 0.14a	-1.22 ± 0.07a	2.89 ± 0.48a	-1.05 ± 0.06a	4.98 ± 1.96a	
		HP	2.51 ± 0.03a	-1.23 ± 0.08a	3.60 ± 0.36a	-1.15 ± 0.03a	10.31 ± 8.25a	
Winter wheat	II	LP	2.36 ± 0.11b	-1.17 ± 0.04a	5.32 ± 0.46a	-1.09 ± 0.07a	7.41 ± 0.27b	
		HP	2.71 ± 0.12a	-1.23 ± 0.04b	5.23 ± 0.51a	-1.11 ± 0.05a	10.67 ± 2.06a	
	III	LP	2.34 ± 0.07b	-1.17 ± 0.01a	4.16 ± 0.54b	-0.98 ± 0.09a	6.06 ± 1.61a	
		HP	2.82 ± 0.11a	-1.22 ± 0.01b	5.49 ± 0.59a	-1.14 ± 0.04b	6.84 ± 1.86a	
	IV	LP	2.50 ± 0.13b	-1.16 ± 0.03a	3.40 ± 0.23b	-0.96 ± 0.02a	3.23 ± 0.08b	
		HP	2.80 ± 0.12a	-1.23 ± 0.02b	5.06 ± 0.17a	-1.15 ± 0.01b	4.79 ± 0.53a	
	V	LP	2.37 ± 0.13b	-1.20 ± 0.02a	3.95 ± 0.07b	-1.01 ± 0a	12.26 ± 2.89a	
		HP	3.01 ± 0.12a	-1.25 ± 0.01a	4.80 ± 0.03a	-1.14 ± 0b	4.89 ± 0.35a	
	Analysis of variance (F value)	Crop (C)		12.38*	0.78	253.82**	3.24	2.62
		Period (P)		59.75**	19.66**	62.86**	36.40**	0.22
HI <sub>d</sub> (H)			6.43*	3.28*	13.34**	2.11	6.02**	
C × P			26.03**	0.16	0.8	3.11	0.95	
C × H			5.06*	4.74*	2.97	0.06	0.82	
P × H			3.03*	0.9	6.09*	10.30**	3.42*	
C × P × H			0.02	1.98	8.45*	0.56	0.43	

extent by influencing hydro-meteorological factors. Indeed, the selected teleconnection factors were crucial for investigating the drought propagation on the large time scale in this study. Furthermore, the temporal changes in the teleconnection factors directly influenced the regional anomalies of the meteorological variables, changing the drought propagation time (Zhang et al. 2022). In addition, increased temperature can enhance actual evapotranspiration (F. Wang et al. 2022a, b), thereby increasing AD frequencies.

### Influences of human activities on the drought propagation from meteorological to agricultural droughts

According to previous related studies, human activities are the main factors contributing to the intensification of AD events (Raposo et al. 2023; Sun et al. 2023; F. Wang et al. 2022a, b). Indeed, human activities, including land use type changes and water consumption for irrigation, domestic, and industrial purposes, can alter the streamflow in rivers and, consequently, restrict water supplies. For instance, the implementation of the “Grain for Green” program increased vegetation cover on steep slopes in the YRB (Jian et al. 2022). In addition, this implementation significantly reduced

streamflow by intercepting rainwater, improving soil structure (Zhang et al. 2023). Hence, under the occurrence of an AD event, these measures may prolong the drought durations in areas with spring wheat cultivations. Agriculture is the largest user of fresh water, accounting for 80% of total water withdrawals. In addition, irrigated land accounts for 45.8% of the total cropland in the YRB (Omer et al. 2021), of which winter wheat is the major crop species. Winter wheat generally had a higher dependence on irrigation practices. Therefore, the occurrence of MD events under insufficient irrigation water amounts may rapidly lead to AD events for winter wheat when compared with spring wheat. Most high precipitation amounts occur in areas with winter wheat cultivations. Hence, the occurrence of drought events in non-growing seasons may be exacerbated by human activities in winter wheat regions (Zhang et al. 2023) and, consequently, reduce irrigation water amounts for winter wheat, thereby leading to AD events during growing seasons.

### Limitations and future directions

The findings of this study demonstrated the suitability of the proposed method by Wang et al. (2021) to qualitatively analyze the influences of climate change and human activities

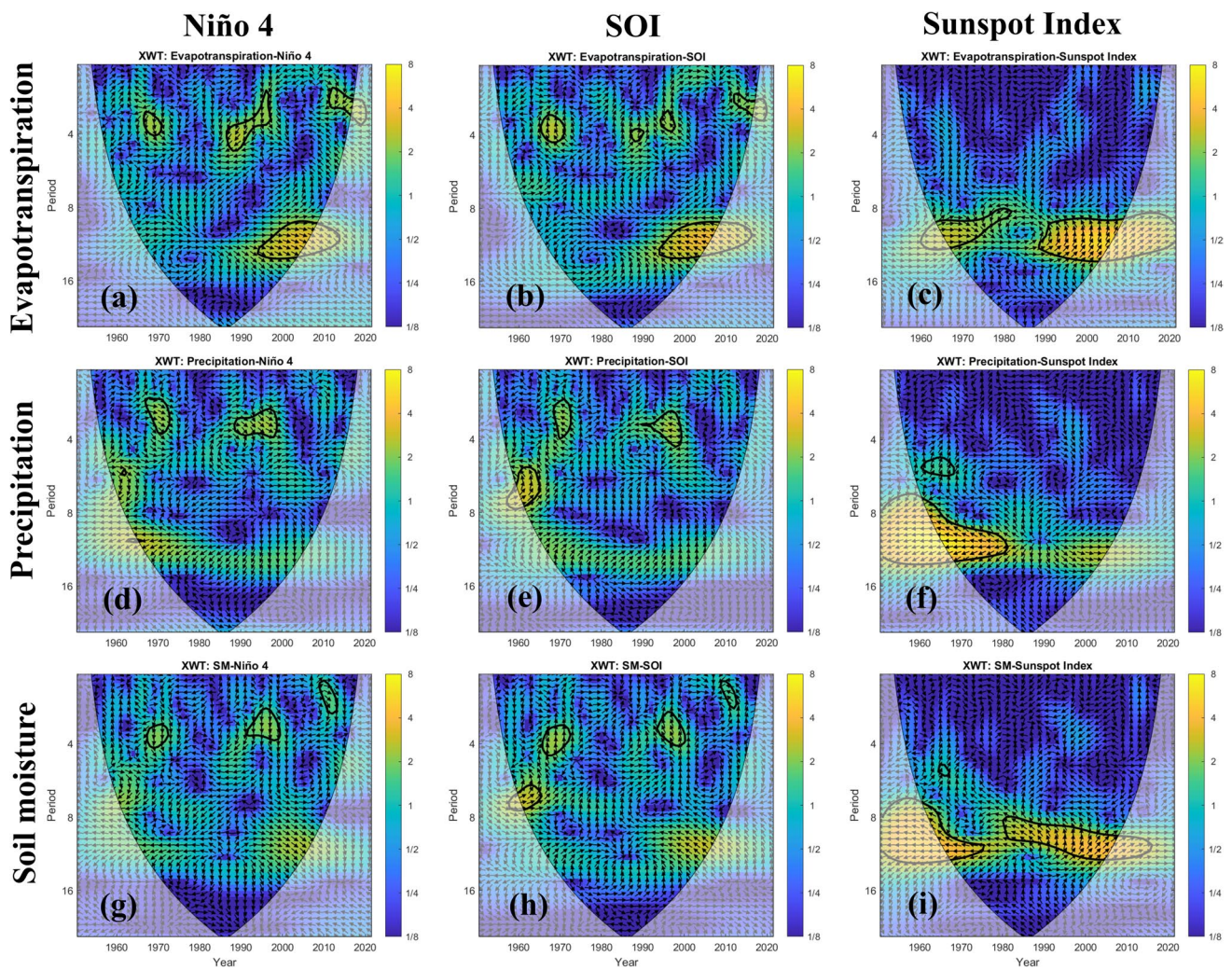


**Fig. 12** The cross wavelet transforms between Niño 4 SST Index, Southern Oscillation Index (SOI), and Sunspot Index, and evapotranspiration, precipitation, and soil moisture (SM) for winter wheat in the Yellow River Basin

on drought characteristics and propagation times. Similarly to our study, previous research has highlighted spatial inhomogeneities of regional climate and catchment properties in some basins (Barker et al. 2016; Jiang et al. 2020). The human activity intensities in catchment areas were subjectively determined in this study, resulting in the lack of substantial differences in the influences of human activities on the drought characteristics and propagation at the defined intensities. The variations in the climate and catchment properties between the selected catchments did not result in notable spatial differences in the drought characteristics and propagation, which can be attributed to the gradual changing nature of drought events. The results of the dynamic drought characteristics and propagation time from MD to AD might be due to the progressive evolution of climatic changes and the increased human activity degrees. Therefore, the classification of the entire study period into different sub-periods

provided significant differences of drought propagation features. The drought propagation model should be used to reveal potential gradual changes in relationships between MD and AD, taking into account the potential influences of the teleconnection factors on large-scale drought conditions.

The present study has some limitations that should be addressed in future-related research. First, the determination of the degrees of human activity impacts degrees and its associated drought propagation requires a large amount of data. In addition, assessment studies on natural and anthropogenic effects on catchment areas require a great deal of information. Consistent study datasets are also required to obtain reliable results. This study analyzed the MD and AD events during spring and winter wheat growth periods without comprehensively revealing the potential relationship between drought characteristics and propagation. Therefore, it is important to analyze the drought index at

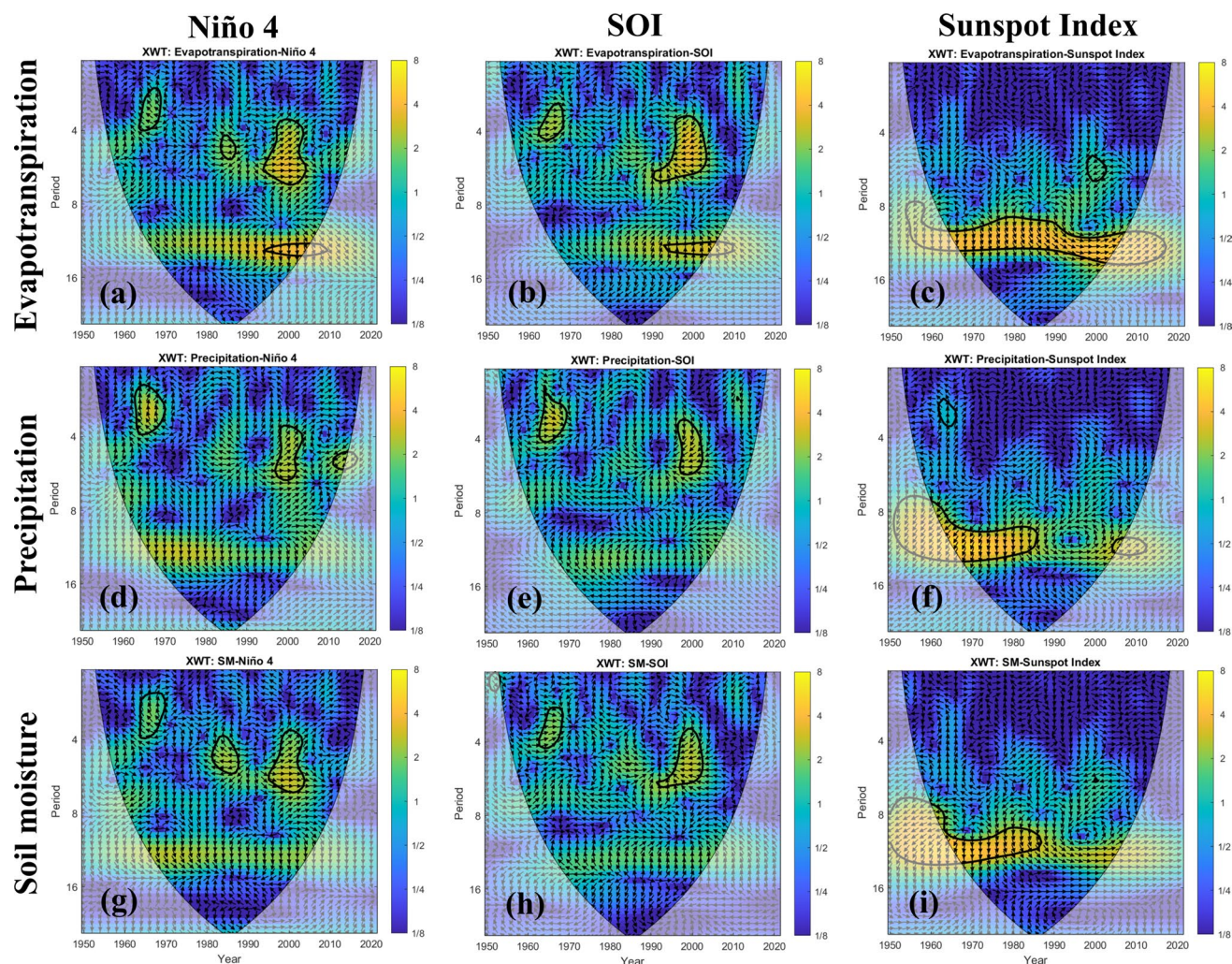


**Fig. 13** The cross wavelet transforms between Niño 4 SST Index, Southern Oscillation Index (SOI), and Sunspot Index, and evapotranspiration, precipitation, and soil moisture (SM) for spring wheat in the Yellow River Basin

a smaller timescale (e.g., weekly and daily timescales) to quantify the relationship between drought characteristics and propagation. Such studies are of great importance for the implementation of effective early AD warning and mitigation strategies. Second, the selection process of catchments without considering the influences of human activities on agricultural drought propagation is very complex and may not be accurate. In this study, an indicator-based score system was employed to determine the comprehensive scores of human activity influence (Table 2 and Fig. 4a). In addition, the catchments were classified based on the score range and factors (GDP, population density, and land use) variation analysis. We suggest future-related research, taking into account more comprehensive factors (e.g., regional CO<sub>2</sub> emissions and industrial structures) in the indicator-based system to propose standard classification criteria of catchments and quantitatively assess natural and anthropogenic impacts on agricultural drought propagation.

Topographic and land cover features may also contribute to drought propagation (Barker et al. 2016; Vicente-Serrano et al. 2004). Indeed, topographic features can influence water storage capacities, leading to different drought propagation times, whereas land cover types can exhibit significant drought tolerance levels, of which forests are the least sensitive to drought events, followed, respectively, by cropland and grassland (Shi et al. 2022). In this study, we investigated drought propagation in dryland at the 0.1° spatial resolution. However, some grid pixels covered forest, grassland, and cropland, which might result in different drought characteristics and propagation times from those in actual cropland. In addition, the presence of forest pixels might underestimate the drought intensity and overestimate the propagation time, while those of grassland might overestimate the drought intensity and underestimate the propagation time. Therefore, further studies on AD investigated are required, taking into account topographic factors and smaller grid pixels.

## Conclusions

In this study, we used a modified observation-based natural and human-impacted catchment comparison method to quantitatively analyze the influences of climate change and human activities on drought characteristics and propagation from meteorological to AD. The Yellow River Basin (YRB) catchments were divided into different Hid degrees based on the comprehensive human influence scores. In addition, the entire research period was categorized into different sub-periods using the heuristic segmentation method, namely the NP (without impacts of human activities), LP (with low impact of human activities), and HP (with high impact of human activities), corresponding to 1950–1971, 1972–1995, and 1996–2021, respectively.

The results of the MD characteristics in the YRB showed a drying trend, particularly in areas with winter wheat cultivations. On the other hand, reduced MDI values were observed in catchments with higher human influence degree (Hid). Most catchments displayed a significant drying trend of the AD events. In addition, the AD trends for winter wheat are expected to be worse than those for spring wheat without significant changing trends of the Hid. The results showed increasing trends of the MDI under Hid-I, Hid-II, and Hid-III in areas with spring wheat cultivations. On the other hand, the ADI under Hid-I, Hid-II, and Hid-III showed increasing trends in the NP followed by those in the LP and HP. The ADI under the lowest and highest Hid displayed increasing–decreasing trends in areas with winter wheat cultivations. In contrast, stable variation patterns of the ADI were observed under the other Hids. The dynamic MDI values showed statistically insignificant decreasing trends under most Hids in areas with spring and winter wheat cultivations. In contrast, the dynamic ADI values exhibited a significant decreasing trend ( $p < 0.01$ ), with a higher changing rate than those of the MDI.

The drought propagation time ranged from 0 to 20 months in all sub-periods and areas with spring and winter wheat cultivations. The higher inconsistent propagation time was observed in areas with spring wheat cultivations in all catchments and under all Hids. The most prolonged drought propagation time was observed in almost all catchments with spring and winter wheat cultivations and under all Hids in the NP, followed by those in the LP and HP. The critical winter and spring growth periods showed prolonged propagation times in the April–May and June–July periods, respectively, demonstrating the positive role of human activities in ensuring optimal soil moisture contents for crop growth. Only three Hids (Hid-II and Hid-V for winter wheat and Hid-I for spring wheat) showed insignificant increasing trends of the

drought propagation time. In contrast, the remaining Hids demonstrated statistically significant increasing trends of the drought propagation time in the YRB.

In this study, three comparison scenarios were considered to assess the impacts of climate change and human activities on drought characteristics and propagation in areas with spring and winter wheat cultivations. In scenario I, the drought propagation features of catchments were analyzed under all Hids in the NP, while the consistency of different Hids for MD and AD characteristics and propagation times was established. The results showed a lower changing rate of the MDI had lower than that of the ADI. In addition, the propagation time from MD to AD was shorter than 10 months in both spring and winter wheat areas. In scenario II, the drought propagation features of the catchment areas minimally impacted by human influences were analyzed in all sub-periods. In addition, the climate change influences on the drought characteristics and propagation times in spring and winter wheat areas were also investigated. The results showed higher increasing rates of the MDI and ADI in spring wheat areas with Hid-I and winter wheat areas with Hid-II in the NP, followed by those in the LP and HP. On the other hand, the corresponding propagation times were shortened under the influences of climate change. In scenario III, the observed results in all catchments during the LP and HP were first analyzed before investigating the influences of human activities on the drought characteristics and propagation in spring and winter wheat areas. The results showed increased MDI and ADI in spring and winter wheat areas. Furthermore, the corresponding drought propagation times were substantially prolonged in spring and winter wheat areas in the LP as compared with those in the HP under all Hids. The results showed greater fluctuations of the MDI, ADI, and drought propagation time in winter wheat areas than those in spring wheat areas in the HP.

The results demonstrated the suitability of the comparison approach applied to the YRB catchments under the influences of climate change and human activities. Human activities increased AD durations and intensities. The comparison results also revealed that climate change slightly enhanced the drought propagation from MD to AD in the YRB, while human activities significantly disturbed and delayed the propagation process. The results of our study are critical for improving drought prediction accuracies and establishing effective drought management systems.

**Supplementary Information** The online version contains supplementary material available at <https://doi.org/10.1007/s11356-024-32709-z>.

**Acknowledgements** We would like to thank MogoEdit (<https://www.mogoedit.com>) for its English editing during the preparation of this manuscript.

**Author contribution** Liang Li analyzed and interpreted the study data, and wrote the manuscript. Qing Peng analyzed the study data.

Zongyang Li analyzed the study data. Huanjie Cai modified the manuscript and provided the fundings. All authors read and approved the final manuscript.

**Funding** This work was supported by the National Key R&D Program of China (2021YFD1900700) and the National Natural Science of China (52179046).

**Data availability** The datasets used and/or analyzed during the current study are available from the corresponding author on reasonable request.

## Declarations

**Ethics approval** Not applicable.

**Consent to participate** Not applicable.

**Consent to publish** Not applicable.

**Competing interests** The authors declare no competing interests.

## References

- Adnan S, Ullah K, Shuanglin L, Gao S, Khan AH, Mahmood R (2017) Comparison of various drought indices to monitor drought status in Pakistan. *Clim Dyn* 51:1885–1899. <https://doi.org/10.1007/s00382-017-3987-0>
- Adolphi F, Muscheler R, Svensson A, Aldahan A, Possnert G, Beer J, Sjolte J, Björck S, Matthes K, Thiéblemont R (2014) Persistent link between solar activity and Greenland climate during the Last Glacial Maximum. *Nature Geosci* 7:662–666. <https://doi.org/10.1038/ngeo2225>
- Afshar MH, Bulut B, Duzenli E, Amjad M, Yilmaz MT, (2022) Global spatiotemporal consistency between meteorological and soil moisture drought indices. *Agric For Meteorol* 316 <https://doi.org/10.1016/j.agrformet.2022.108848>
- Asadi Zarch MA, Sivakumar B, Sharma A (2015) Droughts in a warming climate: a global assessment of Standardized precipitation index (SPI) and Reconnaissance drought index (RDI). *J Hydrol* 526:183–195. <https://doi.org/10.1016/j.jhydrol.2014.09.071>
- Asong ZE, Wheeler HS, Bonsal B, Razavi S, Kurkute S (2018) Historical drought patterns over Canada and their teleconnections with large-scale climate signals. *Hydrol Earth Syst Sc* 22:3105–3124. <https://doi.org/10.5194/hess-22-3105-2018>
- Ayantobo OO, Li Y, Song S, Yao N (2017) Spatial comparability of drought characteristics and related return periods in mainland China over 1961–2013. *J Hydrol* 550:549–567. <https://doi.org/10.1016/j.jhydrol.2017.05.019>
- Baier K, Duetsch M, Mayer M, Bakels L, Haimberger L, Stohl A (2022) The role of atmospheric transport for El Niño–Southern oscillation teleconnections. *Geophys Res Lett* 49 <https://doi.org/10.1029/2022GL100906>
- Barker LJ, Hannaford J, Chiveron A, Svensson C (2016) From meteorological to hydrological drought using standardised indicators. *Hydrol Earth Syst Sc* 20:2483–2505. <https://doi.org/10.5194/hess-20-2483-2016>
- Behrang Manesh M, Khosravi H, Heydari Alamdarloo E, Saadi Alekasir M, Gholami A, Singh VP (2019) Linkage of agricultural drought with meteorological drought in different climates of Iran. *Theoret Appl Climatol* 138:1025–1033. <https://doi.org/10.1007/s00704-019-02878-w>
- Bernaola-Galvan P, Ivanov PC, Amaral LAN, Goldberger AL, Stanley HE (2001) Scale invariance in the nonstationarity of physiological signals. *Phys Rev Lett* 87:168105. <https://doi.org/10.1103/PhysRevLett.87.168105>
- Bonfils CJW, Santer BD, Fyfe JC, Marvel K, Phillips TJ, Zimmerman SRH (2020) Human influence on joint changes in temperature, rainfall and continental aridity. *Nat Clim Change* 10:726 <https://doi.org/10.1038/s41558-020-0821-1>
- Cao S, Zhang L, He Y, Zhang Y, Chen Y, Yao S, Yang W, Sun Q (2022) Effects and contributions of meteorological drought on agricultural drought under different climatic zones and vegetation types in Northwest China. *Sci Total Environ* 821:153270. <https://doi.org/10.1016/j.scitotenv.2022.153270>
- Chen X, Li F, Wang Y, Feng P, Yang R (2019) Evolution properties between meteorological, agricultural and hydrological droughts and their related driving factors in the Luanhe River basin, China. *Hydrol Res* 50:1096–1119. <https://doi.org/10.2166/nh.2019.141>
- Dai A (2013) Increasing drought under global warming in observations and models. *Nat Clim Chang* 3:52–58. <https://doi.org/10.1038/nclimate1633>
- Dai M, Huang S, Huang Q, Zheng X, Su X, Leng G, Li Z, Guo Y, Fang W, Liu Y (2022) Propagation characteristics and mechanism from meteorological to agricultural drought in various seasons. *J Hydrol* 610:127897. <https://doi.org/10.1016/j.jhydrol.2022.127897>
- Dehghannik M, Kaviani MR, Moazami S (2021) Spatial analysis of meteorological and hydrological drought characteristics using Copula model. *Environ Earth Sci* 80:802. <https://doi.org/10.1007/s12665-021-09868-0>
- Dong H, Li R, Li J, Li S (2020) Study on urban spatiotemporal expansion pattern of three first-class urban agglomerations in China derived from integrated DMSP-OLS and NPP-VIIRS nighttime light data. *J Geogr Inf Syst* 22:1161–1174. <https://doi.org/10.12082/dqxkx.2020.190711>
- Fang W, Huang SZ, Huang Q, Huang GH, Wang H, Leng GY, Wang L (2020) Identifying drought propagation by simultaneously considering linear and nonlinear dependence in the Wei River basin of the Loess Plateau, China. *J Hydrol* 591:125287. <https://doi.org/10.1016/j.jhydrol.2020.125287>
- Gevaert AI, Veldkamp TIE, Ward PJ (2018) The effect of climate type on timescales of drought propagation in an ensemble of global hydrological models. *Hydrol Earth Syst Sc* 22:4649–4665. <https://doi.org/10.5194/hess-22-4649-2018>
- Grinsted A, Moore JC, Jevrejeva S (2004) Application of the cross wavelet transform and wavelet coherence to geophysical time series. *Nonlinear Proc Geoph* 11:561–566. <https://doi.org/10.5194/npg-11-561-2004>
- Gu L, Chen J, Yin J, Sullivan SC, Wang H-M, Guo S, Zhang L, Kim J-S (2020) Projected increases in magnitude and socioeconomic exposure of global droughts in 1.5 and 2 °C warmer climates. *Hydrol Earth Syst Sci* 24:451–472. <https://doi.org/10.5194/hess-24-451-2020>
- Guo W, Huang S, Huang Q, She D, Shi H, Leng G, Li J, Cheng L, Gao Y, Peng J (2023) Precipitation and vegetation transpiration variations dominate the dynamics of agricultural drought characteristics in China. *Sci Total Environ* 898:165480. <https://doi.org/10.1016/j.scitotenv.2023.165480>
- Hamed KH, Ramachandra Rao A (1998) A modified Mann-Kendall trend test for autocorrelated data. *J Hydrol* 204:182–196. [https://doi.org/10.1016/S0022-1694\(97\)00125-X](https://doi.org/10.1016/S0022-1694(97)00125-X)
- Han L, Zhang Q, Zhang Z, Jia J, Wang Y, Huang T, Cheng Y (2021a) Drought area, intensity and frequency changes in China under climate warming, 1961–2014. *J Arid Environ* 193:104596. <https://doi.org/10.1016/j.jaridenv.2021.104596>

- Han X, Zhou Y, Wang S, Liu R, Yao Y (2012) GDP spatialization in China based on DMSP/OLS data and land use data. *Remote Sens Technol* 27:396–405
- Han Z, Huang Q, Huang S, Leng G, Bai Q, Liang H, Wang L, Zhao J, Fang W (2021b) Spatial-temporal dynamics of agricultural drought in the Loess Plateau under a changing environment: characteristics and potential influencing factors. *Agric Water Manag* 244:106540. <https://doi.org/10.1016/j.agwat.2020.106540>
- Han Z, Huang S, Huang Q, Leng G, Wang H, He L, Fang W, Li P (2019) Assessing GRACE-based terrestrial water storage anomalies dynamics at multi-timescales and their correlations with teleconnection factors in Yunnan Province, China. *J Hydrol* 574:836–850. <https://doi.org/10.1016/j.jhydrol.2019.04.093>
- He B, Liu Z, Yang X, Sun S (2017) Temporal and spatial variations of agro-meteorological disasters of main crops in China in a changing climate (II):drought of cereal crops in Northwest China. *Chin J Agrometeorol* 38:31–41
- Huang S, Chang J, Leng G, Huang Q (2015a) Integrated index for drought assessment based on variable fuzzy set theory: a case study in the Yellow River basin, China. *J Hydrol* 527:608–618. <https://doi.org/10.1016/j.jhydrol.2015.05.032>
- Huang S, Huang Q, Chang J, Leng G, Xing L (2015b) The response of agricultural drought to meteorological drought and the influencing factors: a case study in the Wei River Basin, China. *Agric Water Manag* 159:45–54. <https://doi.org/10.1016/j.agwat.2015.05.023>
- Huang S, Zhang X, Chen N, Li B, Ma H, Xu L, Li R, Niyogi D (2021) Drought propagation modification after the construction of the Three Gorges Dam in the Yangtze River Basin. *J Hydrol* 603 <https://doi.org/10.1016/j.jhydrol.2021.127138>
- Jian S, Zhang Q, Wang H (2022) Spatial–temporal trends in and attribution analysis of vegetation change in the Yellow River Basin, China. *Remote Sens* 14:4607. <https://doi.org/10.3390/rs14184607>
- Jiang P, Ding W, Yuan Y, Ye W (2020) Diverse response of vegetation growth to multi-time-scale drought under different soil textures in China's pastoral areas. *J Environ Manage* 274 <https://doi.org/10.1016/j.jenvman.2020.110992>
- Kumar Masanta S, Srinivas VV (2022) Proposal and evaluation of non-stationary versions of SPEI and SDDI based on climate covariates for regional drought analysis. *J Hydrol* 610 <https://doi.org/10.1016/j.jhydrol.2022.127808>
- Li X, Sun J, Jiang X (2022) Yellow River Water Resources Bulletin. Yellow river Conservancy Commission of the Ministry of Water Resources, Zhengzhou, Henan, China
- Liu Z, Wang Y, Shao M, Jia X, Li X (2016) Spatiotemporal analysis of multiscalar drought characteristics across the Loess Plateau of China. *J Hydrol* 534:281–299. <https://doi.org/10.1016/j.jhydrol.2016.01.003>
- Ma T, Zhou C, Pei T, Haynie S, Fan J (2012) Quantitative estimation of urbanization dynamics using time series of DMSP/OLS nighttime light data: a comparative case study from China's cities. *Remote Sens Environ* 124:99–107. <https://doi.org/10.1016/j.rse.2012.04.018>
- Maity R, Suman M, Verma NK (2016) Drought prediction using a wavelet based approach to model the temporal consequences of different types of droughts. *J Hydrol* 539:417–428. <https://doi.org/10.1016/j.jhydrol.2016.05.042>
- Nguyen T-T-H, Li M-H, Vu TM, Chen P-Y (2023) Multiple drought indices and their teleconnections with ENSO in various spatiotemporal scales over the Mekong River Basin. *Sci Total Environ* 854:158589. <https://doi.org/10.1016/j.scitotenv.2022.158589>
- Omer A, Zhuguo M, Yuan X, Zheng Z, Saleem F (2021) A hydrological perspective on drought risk-assessment in the Yellow River Basin under future anthropogenic activities. *J Environ Manage* 289:112429. <https://doi.org/10.1016/j.jenvman.2021.112429>
- Park C-E, Jeong S-J, Joshi M, Osborn TJ, Ho C-H, Piao S, Chen D, Liu J, Yang H, Park H, Feng S (2018) Keeping global warming within 1.5°C constrains emergence of aridification. *Nature Clim Change* 8:70–74. <https://doi.org/10.1038/s41558-017-0034-4>
- Perkl RM (2017) Measuring landscape integrity (LI): development of a hybrid methodology for planning applications. *J Environ Planning Manage* 60:92–114. <https://doi.org/10.1080/09640568.2016.1142863>
- Rangecroft S, Van Loon AF, Maureira H, Verbist K, Hannah DM (2019) An observation-based method to quantify the human influence on hydrological drought: upstream–downstream comparison. *Hydrol Sci J* 64:276–287. <https://doi.org/10.1080/02626667.2019.1581365>
- Raposo VDMB, Costa VAF, Rodrigues AF (2023) A review of recent developments on drought characterization, propagation, and influential factors. *Sci Total Environ* 898:165550. <https://doi.org/10.1016/j.scitotenv.2023.165550>
- Samaniego L, Thober S, Kumar R, Wanders N, Rakovec O, Pan M, Zink M, Sheffield J, Wood EF, Marx A (2018) Anthropogenic warming exacerbates European soil moisture droughts. *Nat Clim Change* 8:421. <https://doi.org/10.1038/s41558-018-0138-5>
- Sanderson EW, Jaiteh M, Levy MA, Redford KH, Wannebo AV, Woolmer G (2002) The human footprint and the last of the wild. *Bioscience* 52:891. [https://doi.org/10.1641/0006-3568\(2002\)052\[0891:THFATL\]2.0.CO;2](https://doi.org/10.1641/0006-3568(2002)052[0891:THFATL]2.0.CO;2)
- Shao X, Yan C (2007) Study on the pattern of water requirements of main crops and rainfall in the Yellow River Basin. *Chin J Agrometeorol* 40–44
- Shi X, Ding H, Wu M, Zhang N, Shi M, Chen F, Li Y (2022) Effects of different types of drought on vegetation in Huang-Huai-Hai River Basin. *China Ecological Indicators* 144:109428. <https://doi.org/10.1016/j.ecolind.2022.109428>
- Singh J, Ashfaq M, Skinner CB, Anderson WB, Mishra V, Singh D (2022a) Enhanced risk of concurrent regional droughts with increased ENSO variability and warming. *Nat Clim Change* 12:163–170. <https://doi.org/10.1038/s41558-021-01276-3>
- Singh U, Agarwal P, Sharma PK (2022b) Meteorological drought analysis with different indices for the Betwa River basin, India. *Theor Appl Climatol* 148:1741–1754. <https://doi.org/10.1007/s00704-022-04027-2>
- Small C, Elvidge CD, Balk D, Montgomery M (2011) Spatial scaling of stable night lights. *Remote Sens Environ* 115:269–280. <https://doi.org/10.1016/j.rse.2010.08.021>
- Spearman C (2010) The proof and measurement of association between two things. *Int J Epidemiol* 39:1137–1150. <https://doi.org/10.1093/ije/dyq191>
- Suman M, Maity R (2021) Assessment of basin-wise future agricultural drought status across India under changing climate. *J Water Clim* 12:2400–2421. <https://doi.org/10.2166/wcc.2021.369>
- Sun P, Liu R, Yao R, Shen H, Bian Y (2023) Responses of agricultural drought to meteorological drought under different climatic zones and vegetation types. *J Hydrol* 619:129305. <https://doi.org/10.1016/j.jhydrol.2023.129305>
- Theobald DM (2010) Estimating natural landscape changes from 1992 to 2030 in the conterminous US. *Landscape Ecol* 25:999–1011. <https://doi.org/10.1007/s10980-010-9484-z>
- McKee TB, Doesken NJ, Kleist J (1993) The relationship of drought frequency and duration to time scales. In: Eighth Conference on Applied Climatology. Anaheim, California pp. 17–22
- Tian Q, Lu J, Chen X (2022) A novel comprehensive agricultural drought index reflecting time lag of soil moisture to meteorology: a case study in the Yangtze River basin, China. *Catena* 209 <https://doi.org/10.1016/j.catena.2021.105804>
- Van Langen SCH, Costa AC, Ribeiro Neto GG, van Oel PR (2021) Effect of a reservoir network on drought propagation in a semi-arid catchment in Brazil. *Hydrol Sci J* 66:1567–1583. <https://doi.org/10.1080/02626667.2021.1955891>

- Van Loon AF (2015) Hydrological drought explained. *Wiley Interdiscip Rev Water* 2:359–392. <https://doi.org/10.1002/wat2.1085>
- Van Loon AF, Van Lanen HAJ (2012) A process-based typology of hydrological drought. *Hydrol Earth Syst Sc* 16:1915–1946. <https://doi.org/10.5194/hess-16-1915-2012>
- Vicente-Serrano SM, Beguería S, López-Moreno JI (2010) A multiscalar drought index sensitive to global warming: the Standardized Precipitation Evapotranspiration Index. *J Clim* 23:1696–1718. <https://doi.org/10.1175/2009jcli2909.1>
- Vicente-Serrano SM, Gonzalez-Hidalgo JC, de Luis M, Raventos J (2004) Drought patterns in the Mediterranean area: the Valencia region (eastern Spain). *Climate Res* 26:5–15. <https://doi.org/10.3354/cr026005>
- Wang F, Lai H, Li Y, Feng K, Zhang Z, Tian Q, Zhu X, Yang H (2022a) Dynamic variation of meteorological drought and its relationships with agricultural drought across China. *Agric Water Manag* 261:107301. <https://doi.org/10.1016/j.agwat.2021.107301>
- Wang F, Wang Z, Yang H, Zhao Y, Li Z, Wu J (2018) Capability of remotely sensed drought indices for representing the spatio-temporal variations of the meteorological droughts in the Yellow River Basin. *Remote Sens* 10. <https://doi.org/10.3390/rs10111834>
- Wang M, Jiang S, Ren L, Xu C-Y, Menzel L, Yuan F, Xu Q, Liu Y, Yang X (2021) Separating the effects of climate change and human activities on drought propagation via a natural and human-impacted catchment comparison method. *J Hydrol* 603. <https://doi.org/10.1016/j.jhydrol.2021.126913>
- Wang Y, Wang S, Zhao W, Liu Y (2022b) The increasing contribution of potential evapotranspiration to severe droughts in the Yellow River basin. *J Hydrol* 605:127310. <https://doi.org/10.1016/j.jhydrol.2021.127310>
- Wang Z, Li J, Lai C, Zeng Z, Zhong R, Chen X, Zhou X, Wang M (2017) Does drought in China show a significant decreasing trend from 1961 to 2009? *Sci Total Environ* 579:314–324. <https://doi.org/10.1016/j.scitotenv.2016.11.098>
- Williams AP, Cook ER, Smerdon JE, Cook BI, Abatzoglou JT, Bolles K, Bark SH, Badger AM, Livneh B (2020) Large contribution from anthropogenic warming to an emerging North American megadrought. *Science* 368:314–318
- Woolmer G, Trombulak SC, Ray JC, Doran PJ, Anderson MG, Baldwin RF, Morgan A, Sanderson EW (2008) Rescaling the human footprint: a tool for conservation planning at an ecoregional scale. *Landsc Urban Plan* 87:42–53. <https://doi.org/10.1016/j.landurbplan.2008.04.005>
- Wu G, Chen J, Shi X, Kim J, Xia J, Zhang L (2022) Impacts of global climate warming on meteorological and hydrological droughts and their propagations. *Earth's Future* 10. <https://doi.org/10.1029/2021EF002542>
- Wu J, Chen X, Yao H, Zhang D (2021) Multi-timescale assessment of propagation thresholds from meteorological to hydrological drought. *Sci Total Environ* 765:144232. <https://doi.org/10.1016/j.scitotenv.2020.144232>
- Xie W, Tian H (2011) Study on the application of five drought indexes in Anhui Province. *Meteorol Mon* 37:503–507
- Xu X (2022) China night light annual data set. <https://doi.org/10.12078/2022090902>
- Xu X (2020) China DEM Spatial Distribution Grid Dataset
- Xu X (2017a) China GDP spatial distribution kilometer grid dataset. <https://doi.org/10.12078/2017121102>
- Xu X (2017b) China population spatial distribution kilometer grid dataset. <https://doi.org/10.12078/2017121101>
- Xu X, Liu J, Zhang S, Li R, Yan C, Wu S (2018) China's national land use and cover change data set. <https://doi.org/10.12078/2018070201>
- Xu Y, Zhang X, Hao ZC, Singh VP, Hao FH (2021) Characterization of agricultural drought propagation over China based on bivariate probabilistic quantification. *J. Hydrol* 598. <https://doi.org/10.1016/j.jhydrol.2021.126194>
- Yevjevich V (1967) An objective approach to definitions and investigations of continental hydrologic droughts. *J Hydrol*. [https://doi.org/10.1016/0022-1694\(69\)90110-3](https://doi.org/10.1016/0022-1694(69)90110-3)
- Zhang H, Ding J, Wang Y, Zhou D, Zhu Q (2021) Investigation about the correlation and propagation among meteorological, agricultural and groundwater droughts over humid and arid/semi-arid basins in China. *J Hydrol* 603. <https://doi.org/10.1016/j.jhydrol.2021.127007>
- Zhang Q, Miao C, Guo X, Gou J, Su T (2023) Human activities impact the propagation from meteorological to hydrological drought in the Yellow River Basin, China. *J Hydrol* 623:129752. <https://doi.org/10.1016/j.jhydrol.2023.129752>
- Zhang Q, Peng J, Singh VP, Li J, Chen YD (2014) Spatio-temporal variations of precipitation in arid and semiarid regions of China: the Yellow River basin as a case study. *Global Planet Change* 114:38–49. <https://doi.org/10.1016/j.gloplacha.2014.01.005>
- Zhang X, Hao Z, Singh VP, Zhang Y, Feng S, Xu Y, Hao F (2022) Drought propagation under global warming: characteristics, approaches, processes, and controlling factors. *Sci Total Environ* 838:156021. <https://doi.org/10.1016/j.scitotenv.2022.156021>
- Zhao C, Piao S, Wang X, Huang Y, Ciais P, Elliott J, Huang M, Janssens IA, Li T, Lian X, Liu Y, Müller C, Peng S, Wang T, Zeng Z, Peñuelas J (2017) Plausible rice yield losses under future climate warming. *Nat Plants* 3:16202. <https://doi.org/10.1038/nplants.2016.202>
- Zhao F, Wang X, Ma S, Wu Y, Qiu L, Sun P, Li Q (2023) Widespread increasing ecosystem water limitation during the past three decades in the Yellow River Basin, China. *JGR Biogeosciences* 128. <https://doi.org/10.1029/2022JG007140>
- Zhao G, Tian P, Mu X, Jiao J, Wang F, Gao P (2014) Quantifying the impact of climate variability and human activities on streamflow in the middle reaches of the Yellow River basin, China. *J Hydrol* 519:387–398. <https://doi.org/10.1016/j.jhydrol.2014.07.014>
- Zhao X, Xia H, Pan L, Song H, Niu W, Wang R, Li R, Bian X, Guo Y, Qin Y (2021) Drought monitoring over Yellow River Basin from 2003–2019 using reconstructed MODIS land surface temperature in Google Earth Engine. *Remote Sens* 13:3748. <https://doi.org/10.3390/rs13183748>
- Zhou Y, Zhou P, Jin J, Li J (2014) Establishment of hydrological drought index based on source of regional water supply and its application to drought frequency analysis for Kunming. *J Hydraul Eng* 45:1038–1049. <https://doi.org/10.13243/j.cnki.slxh.2014.09.004>

**Publisher's Note** Springer Nature remains neutral with regard to jurisdictional claims in published maps and institutional affiliations.

Springer Nature or its licensor (e.g. a society or other partner) holds exclusive rights to this article under a publishing agreement with the author(s) or other rightsholder(s); author self-archiving of the accepted manuscript version of this article is solely governed by the terms of such publishing agreement and applicable law.